scientific reports

Check for updates

OPEN

Integrated experimental and computational evaluation of *Anagallis foemina* derived terpenoids against carbapenem resistant *Acinetobacter baumannii*

Muhammad Afzal[1], Muhammad Umer Khan[1]✉, Syed Zeeshan Haider Naqvi[1], Muhammad Kashif Munir[2], Hasan Ejaz[3], Muharib Alruwaili[3], Bi Bi Zainab Mazhari[4] & Lienda Bashier Eltayeb[5]

As carbapenem resistance in *Acinetobacter baumannii* continues to rise worldwide, > 74% of clinical isolates are now resistant to carbapenemases. This pathogen has become a critical WHO priority and is associated with approximately 57,000 deaths per year; thus, the need for new antimicrobial agents is urgent. Here, we demonstrate that the ethanolic extract of *Anagallis foemina* Mill. has shown robust activity against MDR *A. baumannii* isolates from tertiary care hospitals. Gas chromatography-mass spectrometry (GC–MS) identified 16 bioactive compounds. Agar well diffusion assays showed an inhibition zone of 20.16 ± 0.29 mm at 15 mg/mL, exceeding that of imipenem (8 mm). The minimum inhibitory concentration (MIC) of 1.25 mg/mL, coupled with a minimum bactericidal concentration (MBC) of 2.5 mg/mL (MBC/MIC ratio = 2.0), indicated potent bactericidal activity. Sub-MIC concentrations inhibited biofilm formation by > 90%. Molecular docking showed moderate predicted binding between α-Terpinen-7-al (DockingScore: −5.4 kcal/mol) and γ-Terpinen-7-al (−5.3 kcal/mol) to OXA-24 β-lactamase. The complicated stability was verified for 100 ns production phases. Molecular dynamics simulations were carried out to confirm the stability of the complex and protein-ligand root mean square deviations (RMSD) of < 2.5 Å were obtained. Computational ADMET analysis revealed favorable drug-like properties, gastrointestinal absorption, and no toxicity risk. These findings identify *A. foemina* derived terpenoids as exploratory natural product leads warranting further investigation through isolated compound bioassays, enzyme kinetics, and cellular studies to validate predicted binding modes and antimicrobial potential against MDR *A. baumannii.*

Keywords Terpinen-7-al, OXA-24 β-lactamase, Mechanism-based inhibition, antimicrobial resistance, *Acinetobacter baumannii*, Biofilm inhibition, Natural product drug discovery, Monoterpenes

Multidrug-resistant (MDR) superbugs have emerged as a foremost global public health issue. *Acinetobacter baumannii* has become a formidable pathogen in healthcare environments, and the WHO has classified it as a critical priority pathogen[1]. *A. baumannii* is a gram-negative coccobacillus, aerobic, non-fermenting, opportunistic pathogen with a fast reproduction rate. They are a significant cause of hospital-acquired infections, which are linked to several deaths in healthcare establishments worldwide[2]. The extensive and inappropriate use of antibiotics has led to the evolution of MDR phenotypes in *A. baumannii*, including pan-drug-resistant strains. *A. baumannii* is a significant pathogen that is associated with a diversity of infections ranging from mild to severe in a variety of conditions such as skin, soft tissues, urinary tract infections (UTIs), and intra-abdominal infections, tracheitis, bacteremia, nosocomial meningitis, and ventilator-associated pneumonia[3,4]. Managing

[1]Institute of Molecular Biology and Biotechnology, The University of Lahore, Lahore, Pakistan. [2]HRI-NIH Research Centre Fatima Jinnah Medical University, Lahore, Pakistan. [3]Department of Clinical Laboratory Sciences, College of Applied Medical Sciences, Jouf University, 72388 Sakaka, Saudi Arabia. [4]Department of Clinical Laboratory Sciences, College of Applied Medical Sciences, Jouf University, 75911 Qurayyat, Saudi Arabia. [5]Department of Medical Laboratory Sciences, College of Applied Medical Sciences, Prince Sattam Bin AbdulAziz University- Al-Kharj, 11942 Riyadh, Saudi Arabia. ✉email: Muhammad.umer4@mLt.uol.edu.pk

MDR *A. baumannii* is complicated by its profound pathogenicity, which has contributed to the increasing global mortality rate. Immunocompromised patients have a high prevalence of severe MDR infections, and extensively drug-resistant (XDR) patterns may be associated with a history of prolonged hospitalization, mechanical ventilation, and catheterization. Carbapenems are the antibiotics of choice for treating infections caused by MDR *A. baumannii*. However, their previous use has increased carbapenem resistance in recent years. Polymyxin antibiotics are mainly used as the only treatment for MDR *A. baumannii* infections. Nevertheless, their use is considerably limited due to their potential neurotoxicity and nephrotoxicity[5]. Those that resist at least three antibiotic classes belong to the extensively drug-resistant category of *A. baumannii*. Alternatively, a pan-drug-resistant (PDR) subset of XDR variants is resistant to tigecycline and polymyxins. Finally, new antimicrobials were identified, and novel treatment strategies were introduced for XDR isolates[6,7]. *A. baumannii* is a significant organism due to its widespread presence in various environments, particularly on human skin, and its excellent ability to survive on dry surfaces, e.g., hospital bed rails. *A. baumannii* can be transmitted in some healthcare settings, including wound clinics and ICUs. Antimicrobial resistance in *A. baumannii* is due to multiple mechanisms, including altered gene expression and upregulation of MDR pumps, efflux pumps, and RND family members. RNDs are well-known emerging determinants of *A. baumannii* resistance to antibiotics, among which many have been described, such as *Adel*, *ABC*, *Ade IJK*, *and Ade FGH*[8,9]. Given the rise in multidrug-resistant pathogens, there is an urgent need to discover potential antimicrobial agents. Wild plants have long attracted attention for their potential benefits in treating various ailments[10]. Phytochemicals, which are bioactive constituents produced by plants as secondary metabolites, have been increasingly studied for their antimicrobial properties in treating microbial infections[11]. Screening of plant extracts for antimicrobial activity has revealed that higher plants are a promising source of novel anti-infective agents. Numerous secondary metabolites exhibit promising antimicrobial activity against MDR strains, both as standalone agents or in synergism with antibiotic therapy[12,13].

Anagallis foemina Mill., commonly known as blue pimpernel, is a species of flowering plant in the primrose family Primulaceae with a widespread distribution in North America, most of Europe, and much of Asia. This lush green annual plant has adapted to survive in open, dry, nutrient-rich habitats[14]. The plant is erect and can reach 20 cm in height. The stems of the plant are erect, branching, and bright green, and the sessile leaves are arranged in opposite pairs. Currently, there are few pharmacognostic studies on *A. foemina* Mill. concerning its possible biological activity, including its wound-healing properties. The aerial parts of *A. foemina* are used to make a paste for treating lesions and pimples. It is also dispensed as a decoction for occasional internal and systemic infections[15,16]. In a research study, the methanolic extract of *A. foemina* demonstrated antimicrobial activity against *Bacillus subtilis*, *Staphylococcus aureus*, *Escherichia coli*, *Pseudomonas aeruginosa*, and *Candida albicans*. The anti-inflammatory potential of *A. foemina* was also studied by measuring its inhibitory effects on COX-1 and -2 in the presence of prostaglandin E1, induced by superoxide anion radical scavenging in inflammation[17].

GC–MS profiling revealed 16 constituents of *A. foemina* Mill. ethanolic extract. Traditionally, biological evaluation encompasses two complementary strategies: (1) evaluation of the crude extract to ascertain the global bioactivity of all the components associated with this extract and (2) the isolation and evaluation of single compounds for mechanistic understanding. Both approaches provide relevant information: crude extract testing provides insights into synergistic or antagonistic interactions among components and their clinical relevance; individual compound testing can be used to study mechanisms of action and to develop structure-activity relationships[18]. The present study focuses on the evaluation of crude extract antimicrobial activity and can be considered a screening phase before the isolation of individual compounds. Although α-Terpinen-7-al and γ-Terpinen-7-al were present in minor quantities, they were prioritized for *in silico* analysis due to their documented biological relevance[19]. Structurally, terpenoids are a diverse group of natural products derived from isoprene units form the largest group of plant secondary metabolites with over 60,000 characterized structures. The potential of terpenoids is well-documented against bacteria, fungi and viruses, however, terpenoid mechanisms of action against pathogens is not well understood in a large proportion of cases and the journey from *in vitro* studies to their application in medical care is limited[20]. The current investigation is a contribution to this field because it evaluates both crude extract and potential individual components from *A. foemina* for antimicrobial properties and molecular target identification for multidrug-resistant clinical significance. To our knowledge, this is the first extensive study of phytochemical characterization, antimicrobial assays, and advanced computational approaches, such as molecular docking and molecular dynamics simulations, used to reveal the interaction of *A. foemina* phytocompounds and their antimicrobial mode of action against *A. baumannii* β-lactamase targets. In light of the growing carbapenem resistance and the WHO declaration of MDR *A. baumannii* as a critical global threat to human health, the significance of our results, which show the promise of certain *A. foemina*-derived terpenoids as molecular tool templates for the engineering of new classes of anti-infective molecules, is underscored. These results provide a scientifically grounded basis for future research and drug discovery aimed at combating antimicrobial resistance through natural product scaffolds.

Materials and methods

Plant collection and extraction

The aerial parts of *A. foemina* Mill were collected from the surrounding area of the town Mustafa Abad (Lulyani), district Kasur, Punjab, Pakistan (Online Appendix 1). The plant species were classified taxonomically, and a voucher specimen (IUB/Bot/Herb/20240401/347(B) was lodged in the Botany Department, Islamia University, Bahawalpur, Pakistan (Online Appendix 2). Aerial specimens of *A. foemina* Mill. were washed thoroughly, dehydrated in the shade, ground into a fine powder, and stored in sealed bottles. The extract was obtained by merging 20 g of the grinding material with ethanol (100 mL) in a decanter and capping it tightly. After 5 days, the composite was purified from the filter paper, and a syringe filter was used to remove particulate matter. The

isolated extract was then air-dried at 37 °C to obtain a dry residue. Base solutions were prepared by dissolving the dry extract at 100 mg/mL in 1.0% DMSO (v/v). The solutions were then stored in a light-free refrigerator (Supplementary Methods S1).

Phytochemical analysis

Standardized qualitative methods were employed for the biochemical analysis of the ethanolic extract of *A. foemina*[21]. The extract was analyzed for various compounds, including alkaloids, flavonoids, glycosides, tannins, terpenoids, phenols, saponins, coumarins, carbohydrates, fats and oils, anthraquinones, protein sterols, and steroids. A gas chromatograph (Agilent 7890 A) equipped with a GC–MS detection system was used to evaluate the ethanolic extraction of *A. foemina* Mill. (Supplementary Methods S2).

Bacterial strain preparation

A. baumannii cultures were transferred to nutrient agar plates and incubated at 37 °C for 18–24 h. After incubation, 3–4 distinct colonies of bacteria with similar appearance were inoculated into 10 mL of autoclaved Mueller-Hinton broth (MHB) and incubated at 37 °C overnight on a rotary shaker. The turbidity of overnight-incubated MHB was precisely adjusted to a microbial concentration of 0.5 McFarland Standard (approximately 1.0×10^8 CFU/mL) using sterile MHB broth. The medium pH was adjusted to 7.0 to ensure excellent growth conditions and assay reproducibility (Supplementary Result S3).

Evaluation of antibacterial activity

Agar well diffusion assay

For this technique, Autoclaved Mueller Hinton Agar (MHA) media was decanted into 90 mm Petri dish and solidified up to uniform depth of about 4 mm (about 25 mL per plate) in a laminar airflow cabinet. Wells were generated at a 6 mm diameter aseptically by the wide/proximal end of a sterile 1 mL pipette tip, and selected bacteria were inoculated and swabbed over the agar plates[22]. The wells were filled with extracts at concentrations of 20, 10, and 5 mg/mL. An imipenem 10 µg disc was used as a positive control, and 1.0% DMSO (v/v) as a negative control. After 24 h of incubation at 37 °C, the inhibitory zones were measured in mm using a graduated ruler. The assay was performed in three independent biological replicates with technical repeats, as applicable.

Determination of the minimum inhibitory concentration (MIC) by broth microdilution

The MICs of *A. foemina* Mill extract against *A. baumannii* strains were determined using a modified resazurin-based microplate assay using 96-well microtiter plate[23]. Experimental wells (Row A-H, Column 1–3) of a sterile microtiter plate was loaded with 100 µL MHB. *A. foemina* Mill extract (100 µL; 5 mg/mL) was added to row C-1 to C-3, resulting in a final concentration of 2.5 mg/mL. This concentration was diluted across row C through row H for column 1, 2 and 3. At this stage, 100 µL was extracted from the last wells to preserve a residual volume of 100 µL in each well. In addition, to serve as a positive control for each sample, a concentration of 20 µg/mL of imipenem/cilastatin was placed in the wells of the first row (A1-A3). Additionally, MHB was added to the each treated well to achieve a total volume of 190 µL. Similarly, 190 µL of MHB was added to the Row B1–B3 wells to compare the viability of cell growth with that of the extract-treated wells. The bacterial culture was suspended in a saline solution and compared to a 0.5 McFarland standard (approximately 1.0×10^8 CFU/mL). Each well received 10 µL of the bacterial solution. The microtiter plates were incubated at 37 °C for 24 h. The MIC values were determined by adding 30 µL of resazurin solution (2.5 mg/mL) to each well. Subsequently, the samples were incubated for another two hours to facilitate potential color changes. After the incubation period, any color change was observed visually. A change in color from pink to purple indicates cell growth. Wells that did not show any color change and remained blue were assigned a score ≤ the MIC value.

Minimal bactericidal concentrations (MBC)

The Minimal bactericidal concentrations (MBC) is determined by subculturing aliquots from wells or tubes that have no visible growth during the MIC determination assay onto drug-free, non-selective agar plates and incubation in the same conditions (37 °C, 24 h)[24]. The MBC is described as the lowest concentration of an antimicrobial agent that will reduce the viability of the inoculated pathogens by 99.9% (a 3-log reduction) and effectively kill the bacterial population, rather than merely inhibit the growth of the population after 24 h of incubation at 37 °C [25]. During the MBC experiment, a 5 µL sample was taken from each well, yielding the MIC values. Furthermore, broth was taken from two wells above the MIC. The obtained material was spread onto nutrient agar and incubated at 37 °C for 18–24 h. In addition, the number of colonies was enumerated, and the concentration of sample which gives < 10 colonies was taken as value of MBC[26]. The assay was performed in three independent biological replicates with technical repeats, as applicable.

Biofilm inhibition

Qualitative assessment of biofilm formation by the tube method

Approximately 1 mL of an overnight TSB culture was inoculated into sterile glass test tubes and incubated under static conditions at 37 °C for 24 h in order to stimulate biofilm formation as described by O'Toole & Kolter with some modifications[27]. After incubation, the planktonic cells were carefully removed with a pipette by tilting the tubes and removing the culture medium. The tubes were then washed three times with a sterile phosphate buffered saline (PBS, pH 7.0), in order to remove the unattached cells. Tubes were stained with 200 mL, 0.1% (w/v) crystal violet solution, gently rotated to allow the dye to mix throughout the biofilm, and keep at 37 °C for 15–20-min. A biofilm containing Extracellular Polymeric Substances (EPS) reacts with CV dye, binding it, which can be subsequently detected visually. The samples were briefly stained, then washed with distilled water to remove excess stain, and air-dried. The formation of a visible film along the inner walls or at the bottom

of the tubes was confirmed as biofilm. Biofilm formation was visually scored in standardized form, that is as 0 = absent/non-biofilm producer, 1 = weak biofilm producer (barely stained that is at the walls and at the base of the tube) 2 = moderate biofilm producer (clearly visible distinct stain along the walls and at the bottom of the tube) and 3 = strong biofilm producer (heavy stain and a clear film is visible along the inner walls and the liquid-air interface). The formation of rings at the liquid-air interface was not in itself deemed to be biofilm formation.

Qualitative assessment of biofilm formation by Congo red agar assay

Congo Red Agar (CRA) is a selective and differential medium used to quickly obtain qualitative screening results for biofilm-forming bacteria based on the binding of Congo red dye to the polysaccharides in bacterial biofilm extracellular polymeric substances (EPS) resulting in a characteristic black or red color[28]. To prepare the Congo Red Agar, suspend 37 g of Brain Heart Infusion (BHI) agar powder was suspended in 1 L of distilled water in a 2-liter Erlenmeyer flask and autoclave at 121 °C, 15 psi for 15–20 min and cooled to approximately 50 °C. While cooling the BHI agar, dissolve 50 g of analytical grade sucrose in 50 mL of sterile distilled water with a little heat, and then filter-sterilize through a 0.22 µm membrane filter. Separately, 0.8 g of Congo red dye (analytical grade) was dissolved in 100 mL sterile distilled water at 37 °C (not autoclaved, as high temperatures degrade the dye) and filter-sterilized through a 0.22 µm membrane filter. Once the BHI agar cooled to 50 °C, the filter-sterilized sucrose solution was aseptically added, stirred gently, and then the Congo red dye solution was added and thoroughly mixed until uniform, such that the result was uniformly light red or wine colored. The remaining medium was poured into sterile 90 mm Petri dishes to a depth of approximately 4 mm (~ 25mL per plate) and allowed to solidify at room temperature for approximately 20 min before storage. Before use, the plates were visually examined for a uniform light red color, lack of contamination, and proper solidification. For inoculation, the test bacterial isolate was streaked onto the CRA plate using a sterile inoculation loop, and then incubated inverted at 37 °C for 24 h under aerobic conditions. After incubation, the growth pattern had the following interpretations: in the case of black or dark-pigmented, red, or colorless/transparent colonies, they were strong biofilm producers (positive, or true), and in the case of pink or intermediate colored growth, it was equivocal biofilm formation. This method is fast (24–48 h), economically feasible, and has a high throughput potential. However, it has shown limitations, including qualitative output only, high observer subjectivity in color interpretation, and low sensitivity (40–70%) compared to the quantitative tissue culture plate (TCP) method (sensitivity ~ 73–80%)[29].

Evaluation of biofilm inhibition by the crystal violet microtiter plate assay

To investigate the inhibitory effects of the crude extract on biofilm development by the selected strains, *A. baumannii* were grown overnight in MHB. The crystal violet staining retention technique was employed using a flat-bottom microtiter plate with 96 wells. Fresh bacterial inoculum was prepared according to a previously described standard[27]. Wells A1-F1 were filled with 100 µL of MHB, and the same procedure was repeated for the remaining wells. A total of 100 µL of the extract solution (25 mg/mL) was placed into well A1, diluted, and 100 µL was then recollected for the subsequent wells. Briefly, the solution was diluted two-fold until a concentration of 0.976 mg/mL was achieved in the F1 well. The procedure was repeated for the other columns. Row G was the negative control, containing broth without extract and bacteria. Row G served as the positive control, and broth and bacterial inoculum were added to measure and compare turbidity. Next, 90 µL of MHB and 10 µL of bacterial inoculum were dispensed into the desired wells which resulting in a final volume of 200 µL in each well. Subsequently, the microtiter plates were incubated with 37 °C for overnight. Following incubation, the liquid over the sediment was removed, and then each well was rinsed with sterile distilled water to remove the detached cells. After 30 min of fixing and drying at 50 °C, the biofilms were stained for 10 min at 37 °C with 200 µL of a 1% aqueous solution of crystal violet (CV). Wells were washed with sterile distilled water to remove unabsorbed stains. Subsequently, to solubilize the dye, 200 µL of acetic acid (30%) was added to each well and kept at 37 °C for 15 min. Absorbance was determined at 600 nm OD using a microplate reader. The antibiofilm activity of *A. foemina* Mill extract was calculated as follows:

$$Biofilm\ in\ inhibition\ \% = \ (C - B) - (T - B)\,/C - B \times 100$$

B represents the absorbance per well of the negative control (without inoculation of bacteria), C signifies the absorbance per well of the positive control (wells containing bacterial culture as described above and without extract treatment), and T represents the absorbance per well of the extract-treated wells. This activity was performed in three independent biological replicates with technical repeats, as applicable.

Computational analysis of *A. foemina* Mill phytochemicals

Dataset of protein retrieval and preparation

Structural data for the target bacterial protein, OXA-24 β-lactamase from *A. baumannii*, are archived in the Protein Data Bank (PDB) (https://www.rcsb.org/) under PDB ID 6B22. This protein was selected based on its excellent crystallographic properties, with a resolution below 2.5 Å. The protein was first processed using PyMol Molecular Graphics system version 2.4.0[30]. The target β-lactamase enzyme from multidrug-resistant *A. baumannii* was extracted from the Protein Data Bank and prepared in Biovia Discovery Studio 2021. This preparation involved removing non-essential water molecules and co-crystallized ligands, adding hydrogen, fixing bond orders, optimizing the hydrogen-bonding network . To ensure the integrity of the protein structure, it was validated using SAVES v6.0 (https://saves.mbi.ucla.edu/).

Ligands retrieval and preparation

The 16 bioactive compounds were identified using GC–MS analysis of ethanolic extract of *A. foemina* Mill. ethanolic extract (Supplementary Table S1) and prepared for molecular docking using a united stepwise computational pipeline. The three-dimensional (3D) structures of all 16 phytocompounds were downloaded from the PubChem database in SDF structure data file format. A unique identifier (CP-1 to CP-16) was assigned for tracking and provide reference for each compound. The ligand structures were prepared using Biovia Discovery Studio 2021 and PyMol Molecular Graphics system version 2.4.0 using following operations in a single run as follows: (i) from 2D to 3D coordinate geometry, (ii) adding of all hydrogen atoms using the default algorithm, (iii) automatic assignment of bond orders and formal charges based on the chemical connectivity and (iv) enumeration of ionization states and tautomeric forms at a physiological pH using Epik module. This homogeneous preparation was such that there was no covalent adjustment of the ligands that might modify their properties for use in binding calculations under physiological simulating conditions. Following preparation, the ligand files were directly utilized for molecular docking analysis without performing extra refinement steps thereby ensuring reproducibility, eliminating the redundant steps of any software. All final ligand structures were visually inspected for correct protonation state, 3D geometry before docking to ensure the quality of prepared structures[31].

Molecular docking and binding interaction analysis

Molecular docking was conducted using the AutoDock v1.5.7 at the active-site pocket defined by the co-crystallized ligand[32]. Ligand poses were prioritized using docking score and validated by visual inspection of hydrogen bonds, π-π stacking, and hydrophobic interactions. The interaction profile of the docked complex was analyzed in detail in 3D using the Biovia Discovery Studio 2021 (https://discover.3ds.com/discovery-studio-visualizer-download) and PyMol Molecular Graphics system version 2.4.0 (https://www.pymol.org/). The top-ranked pose (lowest docking Score) was selected for molecular dynamics simulation. For the validation of the reliability of our docking methodology in order to allow comparison of the predicted binding strengths of α-Terpinen-7-al and γ-Terpinen-7-al with known ligands, we performed a docking with three well-characterized OXA-24 inhibitors with published experimental data (Supplementary Methods S4).

Prediction of ADMET properties and drug-likeness

The drug-like properties of the selected ligands were predicted by using SwissADME server (http://www.swissadme.ch/) . This is the most efficient computational approach for estimating the drug-likeness of newly synthesized drugs. The *in silico* pharmacokinetics of the phytocompounds obtained from *A. foemina* were determined by using the pkCSM web server (https://biosig.lab.uq.edu.au/pkcsm/)[33,34]. This computational tool utilizes graph-based signatures to evaluate key ADMET (absorption, distribution, metabolism, excretion, and toxicity) properties in five general areas: absorption (seven descriptors), distribution (four descriptors), metabolism (seven descriptors), excretion (two descriptors), and toxicity (ten descriptors).

DFT studies (MESP/HOMO/LUMO analysis)

Density functional theory (DFT) calculations were performed to investigate the electronic structures and reactivity patterns of the two phytocompounds, α-Terpinene-7-al and γ-Terpinene-7-a. This analysis aimed to evaluate the possible antibacterial potential of the compound against multidrug-resistant *A. baumannii*, using previously described methodologies with slight modifications[35,36]. Among these interactions, B3LYP, which combines Becke's three-parameter exchange with the Lee-Yang-Parr correlation, is a highly successful hybrid functional that accurately calculates molecular properties. All quantum chemical computations were performed according to previously described protocols using the Gauss view software 6.0 (https://gaussian.com/) of programs for all computations with standard convergence criteria. The molecular geometries of the compounds were fully optimized in the gas phase using the B3LYP hybrid functional, which combines the B3LYP correlation functional with the Split Valence plus polarization (SVP) basis set. The default convergence criteria were applied to all calculations. These DFT studies rationalized the theoretical antimicrobial activity of the compounds, correlating electronic properties with the observed binding affinities of α-Terpinen-7-al and γ-Terpinen-7-al (−5.4 kcal/mol & -5.3 kcal/mol) against the β-lactamase enzymes of *A. baumannii* via molecular docking calculations. These DFT computations provide theoretical support for the potential use of the compounds as antimicrobial agents by comparing their electronic properties with the observed binding affinities predicted by molecular docking (−5.4 kcal/mol for α-Terpinen-7-al and -5.3 kcal/mol for γ-Terpinen-7-al) to the enzymes of *A. baumannii*.

Molecular dynamics (MD) simulations

MD simulations were performed to assess the dynamic stability of the protein-ligand complexes[37]. The protein was modelled using the ff14SB force field, while the ligands were parameterized using the General Amber Force Field (GAFF) with the antechamber module to obtain the required atomic charges and parameters (AmberTools20 (https://ambermd.org/AmberTools.php)). All systems were prepared using LEaP. The protein-ligand complex was solvated with an explicit TIP3P water model in a truncated octahedral periodic box, where the optimal solvation layer around the solute reached 9.0 Å from the solute to the edge of the box. To compensate for the net positive charge of the system, two counter-ions of chloride (Cl^-) were introduced. Before the simulation, the system underwent a multi-step energy minimization to eliminate bad contacts. In the first stage, the protein-ligand complex was position-restrained, and the energy was minimized along with the solvent and ions. The entire system was then minimized without bounds to achieve relaxation. After minimization, the system was slowly heated from 0 K to 300 K in the NVT ensemble. Subsequently, it was equilibrated at 300 K and a fixed pressure (NPT ensemble) to ensure thermal and density equilibrium. Finally, a 100 ns production MD

simulation was performed for each complex in the NPT ensemble at 300 K and 1 atm. The generated trajectories were analyzed using the CPPTRAJ module of Amber Tools to determine the RMSD (evaluated to measure the overall complex stability), RMSF (indicating flexible residues), and Rg (as a measure of the overall complex compactness during the simulation period) of the complex from specific structural matrices[38].

Calculation of binding-free energy

The binding free energy (ΔGbind) for each complex was calculated using the Molecular Mechanics/Generalized Born Surface Area (MM/GBSA) method implemented in the AmberTools20 (https://ambermd.org/AmberTools.php) to describe the energetic features of the protein-ligand interactions[39,40]. For this calculation, 1,000 frames were evenly extracted from the last 2 ns of the 100 ns production MD simulation trajectory to ensure the analysis was performed on an equilibrated and stable ensemble. The binding free energy was calculated as the difference between the free energy of the protein-ligand complex and the sum of the free energies of the receptor and ligand in solution:

Total binding free energy: *ΔGbind=Gcomplex-Greceptor-Gligand*.

Every term in the equation was obtained by adding the gas-phase molecular mechanics energy (EMM), the solvation-free energy (Gsol), and the entropic contribution (-TΔS).

Free energy decomposition for each species: $G = GMM + Gsolv - T\Delta S$.

The molecular mechanics energy (EMM) includes van der Waals (ΔEvdW) and electrostatic (Eele) contributions.

Molecular mechanics energy terms: *GMM=EvdW+Eelec*.

The solvation-free energy (Gsol) comprises polar (ΔGGB) and nonpolar (ΔGnp) contributions.

Solvation free energy terms: *Gsolv = GGB+Gnp*.

The polar contribution was calculated using the Generalized Born (GB) model, and the nonpolar term of the solvation-free energy was estimated using the solvent-accessible surface area (SASA)[41]. The computationally intensive term entropic (−TΔS) was not explicitly calculated in this study, which is a standard practice in the approach of comparing the relative binding affinities of structurally similar compounds.

Statistical analysis

Each experiment was repeated in three independent biological replicates with technical repeats, at different occasion. The results are presented as mean standard deviation (± SD) to ensure the reliability and the reproducibility of the results. The antimicrobial effects of *A. foemina* ethanolic extract at concentrations of 20, 10, and 5 mg/mL against three clinical MDR *A. baumannii* isolates were assessed with two-way ANOVA. Tukey's Honestly Significant Difference (HSD) post hoc test was used to identify statistically significant differences between the concentration of extracts between bacterial strains. Additionally, paired t-tests were done to compare CFU counts at MIC vs. 2x MIC to show the bactericidal effect (MBC/MIC ratio). All statistical analyses were conducted in IBM SPSS Statistics version 20.0 (Armonk, NY, USA), and p-value of < 0.05 was considered as statistically significant.

Results

Phytochemical profiling and chemical characterization

Biochemical screening of crude ethanolic extract of *A. foemina* Mill. revealed the presence of glycosides, terpenoids, phenols, carbohydrates, fats, and oils. Comprehensive metabolite profiling was performed using GC–MS, and 16 phytochemicals (Supplementary Table S2) were identified and quantified as visualized in the total ion chromatogram (Supplementary Fig. S1). Chemical composition analysis of the extract revealed the presence of fatty acids and their ester derivatives, which accounted for more than half of the total peak area. The metabolites in the highest amounts were 9,12,15-Octadecatrienoic acid, ethyl ester (13.52%), α-linolenic acid (11.48%), n-Hexadecanoic acid (10.80), and Hexadecanoic acid, ethyl ester (9.26%). Diterpene alcohol phytol (8.81%) and conjugated linoleic acid isomers (7.65%) also significantly contributed to the profile. Cycloeucalenol acetate (6.78%) and vitamin E (3.53%) were the important minor constituents. Of interest are two monoterpenoid aldehydes, namely α-Terpinen-7-al and γ-Terpinen-7-al, which, despite their lower percentages of occurrence (1.62% and 1.70%, respectively), are known to have documented biological activities and were further investigated through computational analysis. This extract shows a chemically diverse profile, and both the major fatty acid components and the minor bioactive terpenoids are likely to contribute synergistically to its observed antibacterial potential against MDR *A. baumannii.*

Identification of *A. baumannii* isolates

Antimicrobial susceptibility profiling of clinical A. baumannii isolates

To establish a baseline for antimicrobial resistance and validate the clinical importance of the tested bacterial strains, the susceptibility of three clinical isolates of *A. baumannii* to a panel of seven antibiotics from diverse drug classes was established. The Kirby-Bauer disc diffusion technique and antimicrobial resistance profiles revealed that all isolates exhibited significant multidrug resistance. The results revealed widespread resistance to several antimicrobial agents in the study area. Globally, the high level of resistance of *A. baumannii* to antibiotics of last resort is critical and a specific clinical concern (Table 1, Supplementary Fig. S2). All experimental isolates were resistant to the carbapenem antibiotic imipenem, with inhibition zones ≤ 8 mm. According to standard international definitions of resistance, the isolates were classified based on their resistance patterns.

Confirmation of A. baumannii isolates and molecular typing

To verify the species-level identity of the three clinical isolates tentatively classified biochemically, PCR amplicons of their 16 S rRNA genes were generated and sequenced. Amplification products were assessed by agarose gel electrophoresis, which yielded a clear single band of approximately 1500 base pairs (bp) for each of the three

Isolates	TZP	C	CFM	CIP	IPM	S	DA	Outcome
A. baumannii-1	R	R	R	R	8 mm	R	R	XDR
A. baumannii-2	R	R	R	R	8 mm	R	R	XDR
A. baumannii-3	R	R	R	R	8 mm	R	R	XDR

Table 1. Susceptibility testing to determine antibiotic-resistant bacterial strains by the Kirby-Bauer disc diffusion method with antibiotic discs.

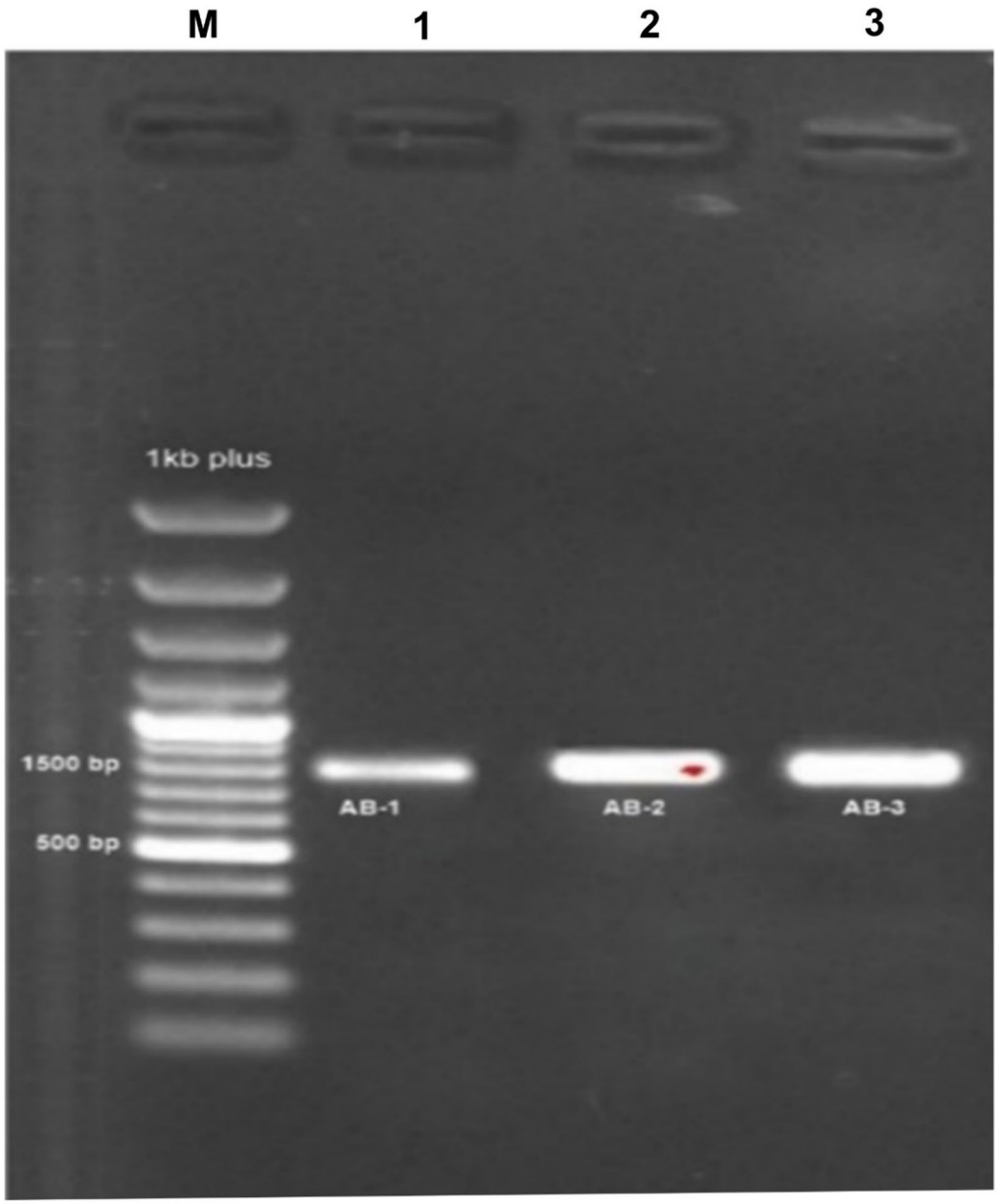

Fig. 1. Amplified PCR products of *A. baumannii* 16 S rRNA.

isolates (Fig. 1). This length is consistent with the known size of the bacterial 16 S rRNA gene and demonstrates successful amplification of the target region. The sequenced amplicons were purified to obtain high-quality 1428–1429 bp nucleotide sequences. These sequences were queried against the GenBank nucleotide database using the Basic Local Alignment Search Tool (BLAST). The sequences showed perfect sequence homology with well-known *A. baumannii* strains (Table 2). Both isolates exhibited ≥ 99% sequence similarity to *A. baumannii* reference sequences, indicating their taxonomic classification. A phylogenetic tree (Supplementary Fig. S3) was

Strain number	Base pair (bp) length	Start in bp	End in bp	Coverage in percentage (%)	Match/Total in	
					Bp	%
AB-1	1429	18	1502	95	1414/1429	99
AB-2	1428	18	1503	95	1413/1428	99
AB-3	1429	19	1502	95	1414/1429	99

Table 2. The table summarizes the sequence alignment data for three *A. baumannii* strains (AB-1 to AB-3), each with a base-pair length of 1528–29 bp.

Bacterial strains	15 mg/mL	10 mg/mL	5 mg/mL	Imipenem (10 µg)
A. baumannii – 1	19.16 ± 0.29	13.83 ± 0.29	No ZI	8 ± 00
A. baumannii – 2	20.83 ± 0.29	13.16 ± 0.29	No ZI	8 ± 00
A. baumannii – 3	18.16 ± 0.29	13.83 ± 0.29	No ZI	8 ± 00

Table 3. Zones of bacterial growth inhibition (mean & SD values in mm) utilizing agar well diffusion assay with the concentrations of *A. foemina* Mill in 20–10 mg/mL and Imipenem at 10 µg.

Factor	F-statistic	*p*-value	η^2 (Effect size)	Interpretation
Concentration Effect (15 vs. 10 mg/mL)	27.45	2.05×10^{-3} **	0.927 (Large)	Highly significant
Strain Effect (Ab-1, Ab-2, Ab-3)	0.87	0.847 (NS)	0.019 (Small)	Nonsignificant
Concentration × Strain Interaction	1.02	0.312 (NS)	0.054 (Small)	Nonsignificant

Table 4. Values represent exact *p*-values of extract concentration (15 vs. 10 mg/mL), bacterial strain (Ab-1, Ab-2, Ab-3), and bacteria*extract interaction; Statistical significance at $\alpha = 0.05$. NS indicates not significant ($p > 0.05$); asterisks indicate significance levels: * $p < 0.05$, ** $p < 0.01$, and *** $p < 0.001$.

generated using the neighbor-joining algorithm and Jukes-Cantor distance model of the MEGA 11 software. Bootstrap analysis was done with 1000 replicates, and the scale bar represents substitutions/site. Bootstrap values were displayed as percentages at nodes and obtained as an indication of the support for each branch. The three clinical isolates (AB-1, AB-2, and AB-3) were grouped together within the major *A. baumannii* clade along with a high bootstrap value (> 87%) included in a clade that is isolated from other *Acinetobacter* species, in accordance with molecular identity. All species names and isolates were clearly labeled with the GenBank accession number of the isolates. Consistent PCR amplification, sequence homology, and phylogenetic sequence placement confirmed the molecular identity of the isolates studied as *A. baumannii*.

Antibacterial activity

Agar well diffusion assay

Antimicrobial efficacy of ethanolic extract of *A. foemina* Mill. was determined using an agar well diffusion assay with three extensively drug-resistant (XDR) *A. baumannii* isolates. The extract exhibited dose-dependent antibacterial activity, with higher concentrations resulting in larger zones of inhibition. At a concentration of 20 mg/mL, the mean inhibition zone diameter of *A. foemina* extract ranged from 18.16 ± 0.29 to 20.83 ± 0.29 mm among the three strains. The inhibition zones formed at 10 mg/mL varied from 13.16 ± 0.29 mm to 13.83 ± 0.29 mm. The 5 mg/mL concentration did not form any inhibition zones. The positive control, imipenem (10 µg), presented a consistent inhibition zone of 8.00 ± 0.00 mm for all tested isolates. In contrast, solvent vehicle blanks showed no antibacterial activity. These results demonstrate that the ethanolic extract of *A. foemina* Mill. exhibited significant antibacterial activity against MDR *A. baumannii* at concentrations of 20 and 10 mg/mL, with effects surpassing those of the positive control antibiotic imipenem (10 µg) (Table 3, Supplementary Figs. S4, S5). The inhibition zone results obtained for the crude extract against MDR *A. baumannii* was comparable in size to the imipenem, positive control. However, a direct quantitative comparison of these measurements is not scientifically meaningful, since the extract (tested as crude material at mg/mL concentrations) and imipenem (tested as a chemically pure compound at µg/mL concentrations in a standardized disc) are fundamentally different in composition, delivery mechanism, and concentration units. Rather than initiating a comparison on the basis of the size of the zones, the observed antimicrobial activity of the crude extract is presented as evidence that bioactivity requires further investigation.

The unit and concentration comparability note are available in Supplementary Methods S1. Two-way ANOVA (Table 4) indicated that the effect of concentration was significant (F (1,4) = 27.45, $p = 2.05*10\text{^}{-3}$, eta-squared = 0.927), indicating that the concentration of the extract was the main factor affecting antibacterial activity. The strain effect was not significant (F (2,4) = 0.87, $p = 0.847$, eta2 = 0.019), indicating uniform susceptibility of the three *A. baumannii* isolates to *A. foemina* treatment. The concentration × strain interaction was also nonsignificant (F (2,4) = 1.02, $p = 0.312$, eta squared = 0.054), confirming that strains did not differ in

their responses to extract concentration. Post-hoc independent-samples t-tests between 15 mg/mL and 10 mg/mL concentrations showed a statistically significant and extremely large effect (t (4) = 7.13, $p = 2.05 * 10^{-3}$, Cohen's d = 5.82), indicating potent dose-dependent inhibition of bacterial growth.

MIC determination

Antimicrobial activity profile of *A. foemina* Mill. extract was systematically evaluated against clinical isolates of *A. baumannii* using a standard microbroth dilution method. In a two-fold serial dilution, the range was recorded from 2.5 mg/mL to 0.078 mg/mL to determine the minimal inhibitory concentration (MIC). Optical density measurements at 600 nm showed concentration-dependent growth inhibition patterns for all tested *A. baumannii* strains. Untreated positive controls maintained an OD of approximately 1.7, whereas negative controls remained clear, indicating reliable antimicrobial test conditions. The MIC of *A. foemina* extract against *A. baumannii* was 1.25 mg/mL, the lowest concentration that inhibited visible bacterial growth after 18–20 h of incubation at 37 °C. Concentrations below 1.25 mg/mL showed reduced activity in a dose-dependent manner, and subordinate bacterial growth was observed at 0.625 mg/mL and below. The resazurin assay supported these observations; wells at or above the MIC were blue, showing inhibited metabolism, and those below the MIC were pink to purple, indicating active bacterial viability (Supplementary Fig. S6). One-way ANOVA confirmed that the tested concentrations of the extract significantly affected bacterial growth (F = 7.517, $p = 0.0001$). The concentration of the extract explained 55.6% of the variation in growth inhibition ($R^2 = 0.5561$).

Post hoc analysis showed that extracts at concentration of 1.25 mg/mL and above had statistically significant growth inhibition as compared to untreated control. The results and methods were validated in three independent replicates.

Determination of MBC

The bactericidal activity of *A. foemina* extract against the three clinical *A. baumannii* isolates is shown in Table 5. A significant reduction in cell viability was seen for all strains at concentrations below MIC of 1.25 mg/mL. However, since viable colonies were recovered (mean CFU counts of 3–5), the extract showed a predominant bacteriostatic effect at this concentration. Similarly, the bactericidal concentration was 2.5 mg/ml (2x MIC). Therefore, the MBC of the *A. foemina* extract was determined to be 2.5 mg/mL. According to the established criteria, when an agent is bactericidal, the MBC/MIC ratio is 4 ≤. The tested extract ratio proves that *A. foemina* is a potent bactericidal agent against *A. baumannii*. This provides good quantitative evidence for antibacterial action against *A. baumannii* rather than merely inhibiting its growth (Supplementary Fig. S7). Paired t-test analysis revealed a significant difference between MIC and 2 × MIC [t (2) = 4.59, $p = 0.044$ (*), large effect size (Cohen's d = 2.65)] for CFU. Critically, the observed MBC/MIC ratio of 2.0 was considerably above the bacteriostatic threshold ratio (> 4) and confirmed the actual bactericidal activity, that confirmed the standards of the FDA and clinical laboratory (Table 5). However, this ratio demonstrates that only a 2-fold increase in concentration over the MIC is necessary to achieve rapid and complete bactericidal activity of the *A. foemina* extract, which makes it one of the most potent antimicrobial agents tested against this pathogen. The bactericidal profiles were similar for both MDR *A. baumannii* isolates, suggesting that the extract activity was not strain dependent.

Antibiofilm formation activity

Qualitative assessment of biofilm formation

Staining patterns and pigmentation of selected *A. baumannii* strains were also established using the Crystal Violet (CV) Screening Assay and the Congo Red Agar (CRA) method, respectively, for biofilm development. All strains were identified as strong biofilm producers by forming a highly stained layer in the CV staining assay and by producing dark pigments on Congo Red Agar media. Analysis of staining intensity and pigmentation patterns revealed greater production of extracellular polymeric substances (EPS) in strong biofilm producers, which contribute to both antimicrobial resistance and sustained *A. baumannii* infections (Fig. 2).

Assessment of antibiofilm formation activity

The crude extract of *A. foemina* exhibited robust antibiofilm activity against XDR clinical *A. baumannii* isolates.

The inhibitory effects were dose-dependent and higher concentrations of extract potentially inhibiting the biofilm formation. The *A. foemina* crude extract was tested at two-fold diluted concentrations ranging from 1.25 to 0.039 mg/mL. The extract showed significant antibiofilm inhibition against the isolates at their corresponding MIC (1.25 mg/mL) with 79.74–92.42% antibiofilm activity against the three tested isolates

Bacterial strain	CFU at MIC (1.25 mg/mL)	CFU at 2× MIC (2.5 mg/mL)	Bacterial killing rate (%)	MBC/MIC ratio
Ab-1	5.00 ± 0.58	1.33 ± 0.29	73.4	2
Ab-2	3.33 ± 0.38	1.33 ± 0.29	60.1	2
Ab-3	3.00 ± 0.35	1.00 ± 0.00	66.7	2
Mean ± SD	3.78 ± 1.15	1.22 ± 0.19	66.7 ± 6.7	2

Table 5. Colony-forming unit (CFU) enumeration that demonstrates bactericidal efficiency. Paired t-test was used between viable bacteria at MIC (1.25 mg/mL) and 2X MIC (2.5 mg/mL, maximum bactericidal concentration of the drug). An MBC/MIC ratio of 2 indicated a bactericidal effect, whereas a ratio > 4 suggested a bacteriostatic effect.

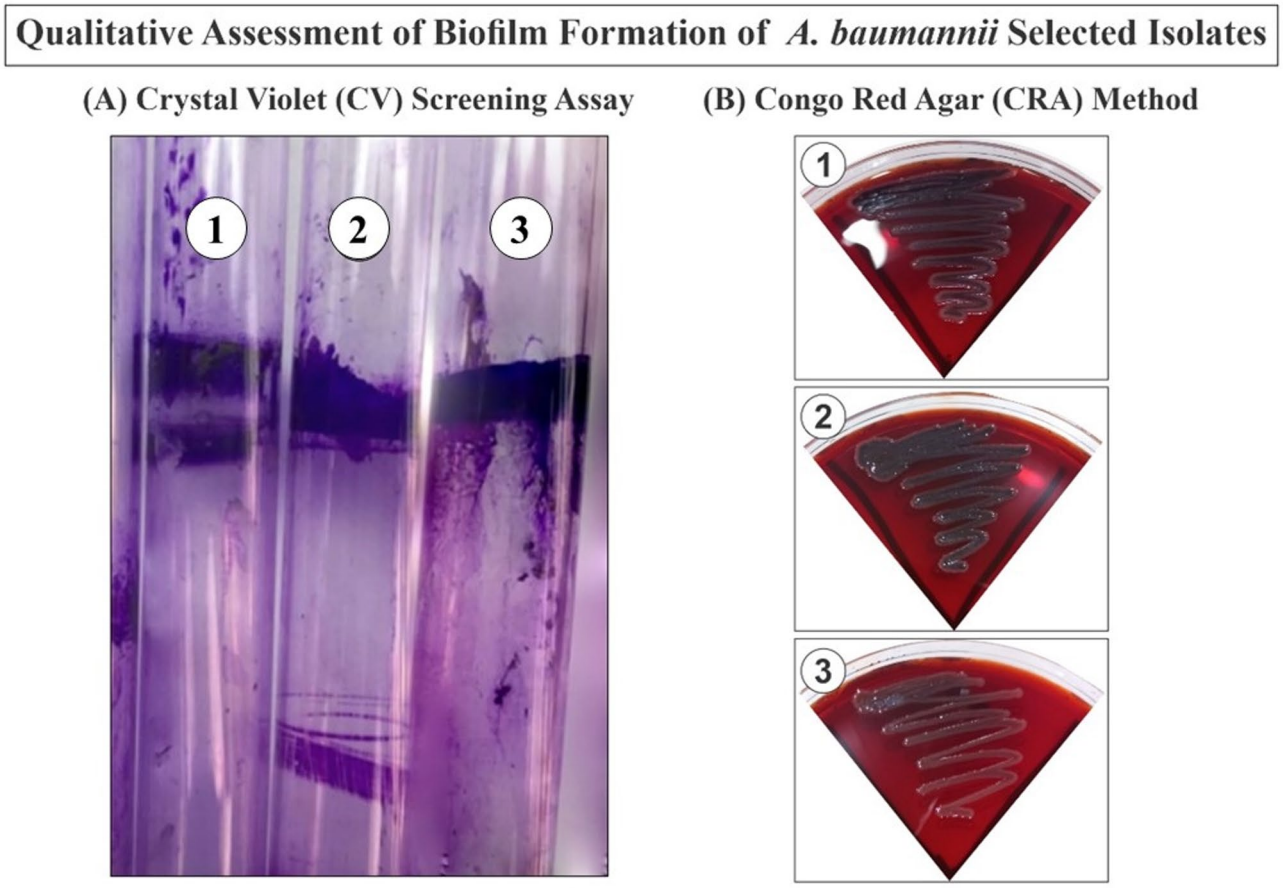

Fig. 2. Biofilm formation screening in *A. baumannii* strains was performed using the (**A**) Crystal Violet (CV) Assay and (**B**) Congo Red Agar (CRA) method. Three strong biofilm-forming experimental strains were shown in slices (Online Appendix 4).

Concentration (mg/mL)	Ab-1 inhibition (%)	Ab-2 inhibition (%)	Ab-3 inhibition (%)	Mean ± SD (%)	% of maximum
1.25 (MIC)	92.42	79.74	87.55	86.57 ± 6.40	100
0.625 (0.5× MIC)	85.3	78.9	81.2	81.80 ± 3.24	94.5
0.312 (0.25× MIC)	72.15	65.3	68.75	68.73 ± 3.43	79.4
0.156 (Sub-MIC)	58.42	52.18	55.3	55.30 ± 3.12	63.9
0.078 (Sub-MIC)	35.26	30.42	32.85	32.84 ± 2.42	37.9
0.039 (Sub-MIC)	18.45	14.52	16.9	16.62 ± 1.98	19.2

Table 6. Crystal violet microtiter plate assay results for dose-dependent antibiofilm activity. One-way analysis of variance confirmed a significant concentration effect: R2 = 0.9667 - log linear regression results.

(Table 6). A serial two-fold dilution of the concentration resulted in a reduction of antibiofilm activity, showing that the effect was concentration-dependent (Fig. 3). Notably, the maximum antibiofilm activity was detected at the MIC value. However, a strong inhibitory effect at sub-inhibitory concentrations was still evident, suggesting that the extract could interfere with biofilm architecture at exposure levels that do not kill planktonic bacteria. Pairwise comparison of the MIC and the lowest concentration tested sub-MIC (0.078 mg/mL) revealed a large difference of 53.7% points of biofilm inhibition (Cohen's d = 13.90, extremely large effect). One-way Analysis of Variance between strains confirmed that the effect on biofilm inhibition was not significant (F = 0.09, $p = 0.914$, eta square = 0.008), indicating a uniform effect across all tested isolates.

In silico studies

In silico validation of β-lactamase protein structure

The computationally modelled β-lactamase was rigorously validated for *in silico* analysis of its structural stability and stereochemical quality. Analysis of the Ramachandran plot displayed a high-quality protein fold, assessing the conformational viability of amino acid residues by their phi (φ) and psi (ψ) dihedral angles. Specifically,

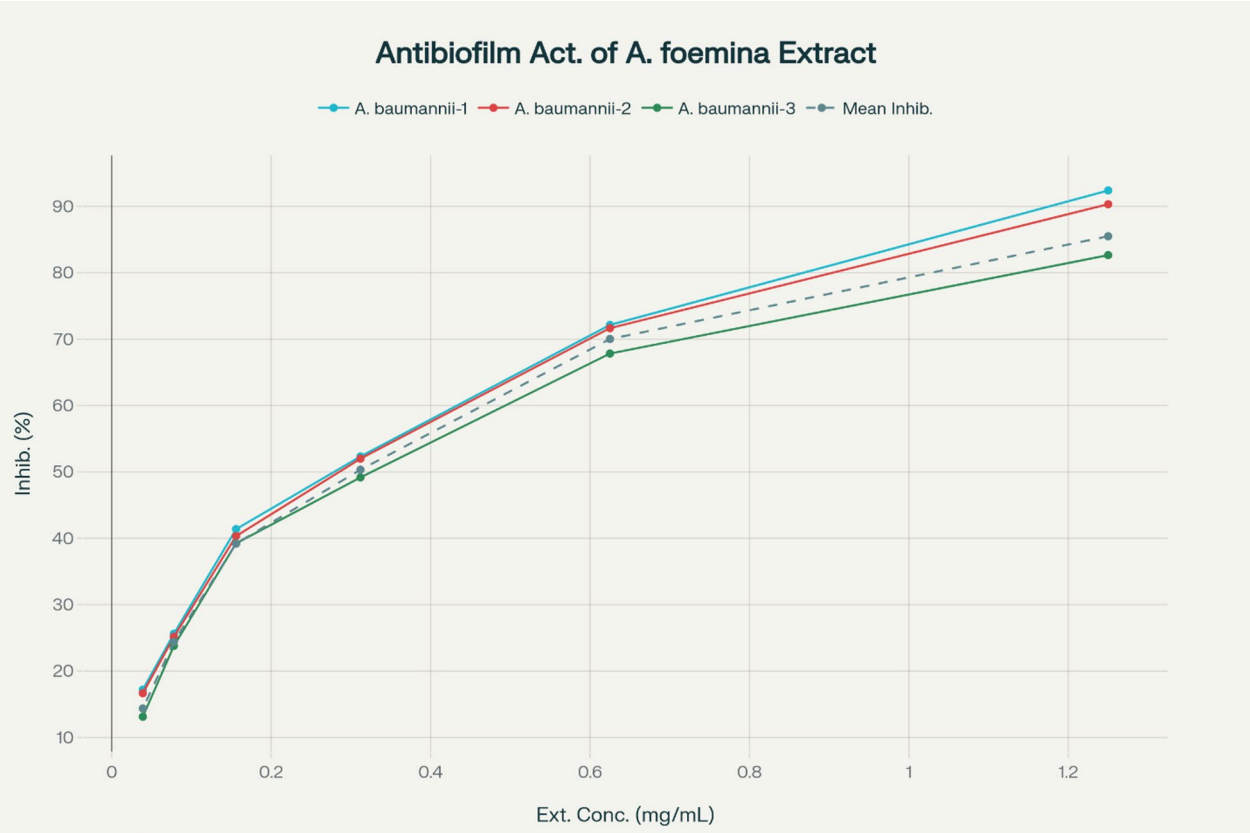

Fig. 3. Inhibition of biofilm formation by *A foemina* crude extract on three *A. baumannii* clinical isolates in a dose-dependent manner.

Validation tool	Parameter	Result	Quality standard & interpretation
Ramachandran Plot	Residues in Most Favorable Regions	94.00%	> 90% (Excellent)
	Residues in Allowed Regions	5.80%	–
	Residues in Disallowed Regions	0.20%	< 0.5% (Excellent)
3D Verification	Overall Structure	Pass	–
ERRAT Score	Overall Quality Factor	> 90	> 90 (High Quality)

Table 7. The table summarizes the important metrics during the validation of the structure model of the β-lactamase protein *in silico*. The Ramachandran plot is a technique used to assess the stereochemical qualities (of the backbone dihedral angles). The ERRAT score is an overall quality of the 3D fold. The quality standards go further to define the thresholds used to classify a high quality, reliable protein model.

94.0% of the residues were located in the plot core (most favorable) regions. An additional 5.8% of residues were positioned in the allowed regions, demonstrating that most of the backbone conformations were sterically allowed. the ramachandran plot showed that 98.6% of the residues were located in the favored regions, with the remaining 0.2% in the disallowed regions (Supplementary Fig. 8). this distribution is consistent with the conclusion that the model is in good structural order, reliable, and free from significant steric clashes and/or problematical conformations. The postulation was confirmed by the ERRAT score, which is a measure of the overall quality of a 3D protein structure and takes into consideration non-bonded interactions between atoms. In this case, the ERRAT score of the model was over 90, indicating a good model structure and well-defined parameters, which is comparable to the method of high-resolution experimental determination (Table 7). This validation showed that the proposed model can be used in additional virtual studies, such as molecular docking simulations, and virtual screening for new inhibitor discovery.

Compound	Docking score (kcal/mol)	Key hydrogen bond residue	Key hydrophobic interaction residues
α-Terpinen-7-al	−5.4	Ser-81, Lys218	Tyr-112, Val-130
γ-Terpinen-7-al	−5.3	Ser-81, Lys218	Tyr-112, Val-130

Table 8. α-Terpinen-7-al exhibits a stronger binding affinity (−5.4 kcal/mol) compared to its γ isomer (−5.3 kcal/mol). Both compounds share a crucial binding mode, forming a key hydrogen bond with the catalytic residue Ser-81. The binding is further stabilized by hydrophobic interactions with residues Tyr-112 and Val-130.

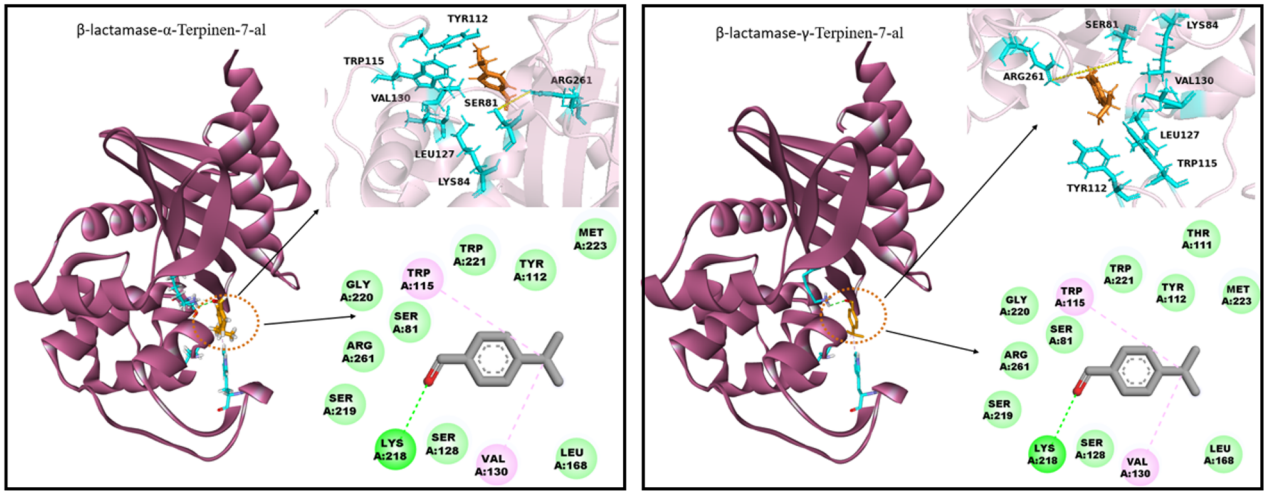

Fig. 4. This image displays the molecular docking of α-Terpinen-7-al (left) and γ-Terpinen-7-al (right) into the active site of *A. baumannii*β-lactamase. Both conformations bind similarly, and the important hydrogen bond to the catalytic residue Ser-81and Lys218 is evident in both 3D and 2D diagrams. Stabilized by hydrophobic contacts with residues such as Tyr-112 and Val-130 this interaction suggests a competitive inhibitory mechanism giving a molecular level insight into their antibacterial activity (Generated using the BIOVIA Discovery Studio Client 2021 version 21.1.0.20298 and PyMol Molecular Graphics system version 2.4.0.

In silico validation of antibacterial docking analyses for *A. baumannii*: interactions of β-lactamase with α-Terpinene-7-al and γ-Terpinene-7-al complexes

To elucidating the structural basis of the observed antibacterial activity, the interacting of the α-Terpinen-7-al and γ-Terpinen-7-al with the β-lactamase enzyme of *A. baumannii* were deciphered using molecular docking simulations. *In silico* docking showed that both phytocompounds would be able to stably accommodate in the active site of the enzyme, with α-Terpinen-7-al binding to a superior extent (docking score = −5.4 kcal/mol) compared to its isomer, γ-Terpinen-7-aL (docking score: −5.3 kcal/mol). An in-depth examination of the best-docked poses showed, that both compounds shared a similar and important binding mode. Both isomers established a key hydrogen bond with the Ser-81 side chain, a catalytic residue of the β-lactamase hydrolytic mechanism. The stability of these ligand-protein complexes was also supported by strong hydrophobic interactions with surrounding nonpolar residues, Tyr-112 and Val-130, which further reinforced their stability. Coupled with these stabilizing hydrophobic contacts, the consistent hydrogen bond with the catalytic serine strongly suggests a precise mechanism for competitive inhibition. This *in silico* evidence provides a robust molecular rationale for the antibacterial activity of these phytochemicals, explaining their potential to neutralize a key resistance mechanism in *A. baumannii* (Table 8; Fig. 4). Molecular docking results and binding affinity of 16 compounds are given in Supplementary Table S3. Characterized OXA-24 inhibitors were used to validate molecular docking (Supplementary Table S4), which shows an important context of the use of molecular docking results for the interpretation of terpenoids binding potential (Supplementary Results S3).

In silico ADMET analysis for drug-likeness and pharmacokinetic potential

To assess the potential of the lead compounds α-Terpinen-7-al and γ-Terpinen-7-al as drug candidates to combat multi-drug resistant *A. baumannii*, the Absorption, Distribution, Metabolism, Excretion and Toxicology (ADMET) profile of the compounds were extensively characterized *in silico* utilizing the reliable computational bioinformatics tools. The pkCSM web server was used to evaluate the synthetic accessibility of both molecules and both were given a score of 1, meaning that they are easily synthesizable. SwissADME (Swiss Institute of Bioinformatics, http://www.swissadme.ch) was used to predict important pharmacokinetic issues, physicochemical properties, drug-likeness and medicinal chemistry properties within a user-friendly environment. Various characteristics of APIs that influence oral bioavailability (intestinal permeability,

Compound	Lipinski's rule compliance	HBA	HBD	Molecular weight (g/mol)	LogP (o/w)
α-Terpinen-7-al	Yes	1	0	150.22	2.26
γ-Terpinen-7-al	Yes	1	0	150.22	2.1

Table 9. Comparison of physicochemical qualities of α-Terpinen-7-al and γ-Terpinen-7-al according to Lipinski's Rule, HBA and HBD, MW and LogP.

Parameter	α-Terpinen-7-al	γ-Terpinen-7-al
Absorption & Distribution		
GI Absorption	High	High
P-gp Substrate	No	No
BBB Penetration	Yes	Yes
Bioavailability Score	0.55	0.55
Log S (SILICOS-IT) (Solubility)	−1.8	−1.8
Metabolism		
CYP1A2 Inhibitor	No	No
CYP2D6 Inhibitor	No	No
CYP2C19 Inhibitor	No	No
CYP2C9 Inhibitor	No	No
CYP3A4 Inhibitor	No	No
Toxicity		
Hepatotoxicity	No	No
AMES Toxicity (Mutagenicity)	No	No
Carcinogenicity	No	No
hERG Inhibition (Cardiotoxicity)	No	No

Table 10. Pharmacokinetic and Toxicology of the Isomers of Terpinen-7-al

lipophilicity, metabolism, excretion, membrane permeation, and toxicology profiles), in terms of physiological factors, were considered. Both phytocompounds fit Lipinski's Rule of Five. They contained molecular weights below 500 g/mol, less than 10 hydrogen bond acceptors (HBA), and less than 5 hydrogen bond donors (HBD) as predicted by SwissADME software, that they exhibit a good pharmacokinetic profile. LogP values of 2.26 for α-Terpinen-7-al, and 2.10 for γ-Terpinen-7-al (LogP (o/w) are calculated and written below) show sufficient lipophilicity for crossing the biological membranes that is basic for a sound absorption and distribution. These *in silico* observations, which are supported by pkCSM (https://biosig.lab.uq.edu.au/pkcsm/) and SwissADME (https://www.swissadme.ch/) calculations, support the drug-likeness of these compounds and give a good rationale for further experimental evaluation of their efficacy and safety profiles (Table 9).

Absorption, distribution, and bioavailability The pharmacokinetic parameters of α-Terpinen-7-al and γ-Terpinen-7-al were calculated *in silico* using the SwissADME and PKCSM programs. These parameters include the Absorption, Distribution, Metabolism, and Bioavailability. Both terpinen isomers had high gastrointestinal (GI) absorption, which shows their potential for oral administration. Neither of these compounds proved to be a substrate for the efflux transporter known as P-glycoprotein (P-gp). This implies a lower risk of cell expulsion from the body and better accumulation in the intracellular compartment, which is very important for *in vivo* therapeutic efficacy. Furthermore, these two compounds are able to cross the blood-brain barrier (BBB) expanding the possibilities for lead generation beyond the periphery. These compounds have moderate systemic availability in spite of a bioavailability score of 0.55, thus making them promising candidates for orally administered drug Development. Their moderate water solubility and Log S (SILICOS-IT) values of −1.80 (both compounds) makes them convenient candidates for drugs with reasonable balance in absorption and distribution for biological systems (Table 10).

Metabolism The metabolic profiles of the two terpenes, α-Terpinen-7-al and γ-Terpinen-7-al, were investigated for their interaction with the cytochrome P450 (CYP) enzyme-system, which is a key determinant factor of the drug metabolism and detoxification in the liver. Understanding a compound's metabolic behavior is very important to its safety and pharmacodynamic (PD) properties. *In silico* analysis revealed that both compounds are not inhibitors of common CYP isoenzymes, i.e., CYP1A2, CYP2D6, CYP2C19, CYP2C9 and CYP3A4. The lack of inhibitory activity is suggestive for a reduced probability of drug-drug interactions which is of major concern in efficacy and safety analysis of a therapy. Furthermore, both compounds showed high levels of metabolic stability, which can be attributed to long-lasting drug effects *in vivo* (Table 10).

Toxicity The toxicological profiles of α-Terpinen-7-al and γ-Terpinen-7-al were investigated, in order to establish the safety of the compounds as drug candidates. An *in silico* study predicted that there was no indication of carcinogenicity, liver damage or mutagenicity for the Ames test, a commonly accepted method for testing the mutagenic potential of chemicals. These naturally occurring compounds have been obtained from A. foemina and lack signals of toxicity and aid in their safety for further development. Moreover, neither compound 2 showed hazard of cardiotoxicity, including hERG channels blocking, confirming their good safety profiles. These data suggest that the phytocompounds could be selected for further drug development for therapeutic purposes such as central nervous system activity, solubility, and metabolic considerations (Table 10).

Frontier molecular orbital energies and molecular electrostatic potential maps of α- and γ-Terpinen-7-al (DFT Analysis)

The electronic structures and reactivities of α-Terpinen-7-al and γ-Terpinen-7-al were systematically investigated using density functional theory (DFT) calculations. This approach gave the key quantum chemical descriptors, e.g., the energy of the Highest Occupied Molecular Orbital (HOMO) and Lowest Unoccupied Molecular Orbital (LUMO) levels. These are worthwhile in order to obtain knowledge about the electronic properties of the elements that are responsible for their molecular interactions with biological targets, such as the β-lactamase enzyme of multidrug-resistant *A. baumannii.* The HOMO energy is the energy associated with the ability of the molecule to donate electrons and the LUMO energy is the energy associated with the ability of the molecule to accept electrons. Lower values of Delta E are associated with higher reactivity and a higher probability of electrons transfer for biological interaction. DFT analysis revealed that the HOMO energy, LUMO energy and HOMO-LUMO energy gap (DE) of α-Terpinen-7-al were 0.021922 eV, 0.06463 eV and 0.42708 eV, respectively.

In comparison, the HOMO energy was 0.020062 eV for γ-Terpen-7-al and the energy gap was 0.41076 eV and the LUMO energy was 0.06145 eV. The small difference in energies in both compounds reflects the high chemical reactivity, which could be important to enable electron-transfer reactions in order to appropriately inhibit the bacterial enzymes. Additionally, molecular electrostatic potential (MESP) surfaces showed electrophilic and nucleophilic regions in both the isomers which has helped to identify interaction binding for the interaction with β-lactamase. The DFT-based electronic properties were consistent with molecular docking, which revealed that α-Terpinen-7-al (−5.4 kcal/mol) and γ-Terpinen-7-al (−5.3 kcal/mol) have favorable binding affinities with *A. baumannii.* Collectively, these results support both compounds as potential lead structures for further optimization as antimicrobial agents against multidrug-resistant pathogens (Table 11; Fig. 5).

In silico validation of MD simulation results

To analyze the stability and binding dynamics of α-Terpinen-7-al and γ-Terpinen-7-al with the multidrug-resistant *A. baumannii* β-lactamase enzyme, the top-ranked dock poses were utilized to perform 100-nanosecond (ns) molecular dynamics (MD) simulations. Explicit solvent simulations were performed under periodic boundary conditions to model physiological conditions using the AMBER force field and the TIP3P water model. The conformational stability of the protein-ligand complexes during the simulations was analyzed by calculating the Root Mean Square Deviation (RMSD) relative to the initial docked conformation. In the case of the β-lactamase-α-Terpinen-7-al complex, the average RMSD (protein backbone and ligand) remained steady from 0.5 to 2.5 Å (mean: 1.5 ± 0.3 Å). This narrow range suggests the low structural divergence and stable binding which indicate strong interactions between the ligand and the activating site. The overall structural stability of the complex was maintained over the 100 ns simulation and some fluctuations occurred in the flexible loop regions and solvent exposed domains, which is not unusual for MD simulations and are much like local conformational rearrangements and do not indicate global destabilization (Fig. 6Panel A).

In contrast, the fluctuations of RMSD of the complex between the molecule and the solvent, i.e., the compound of the β-lactamase and γ-Terpinen-7-al, had values ranging from 0.5 to 2.0 Å over a total time period of 100 ns. This RMSD indicates a stable binding pose (Fig. 6Panel B). These results, emphasize the plasticity of the ligand-enzyme interaction, and the importance of additional investigation (e.g., binding free energy calculations with techniques such as MM-PBSA and per-residue interaction profiling) for the *in silico* validation of the long-term stability and specificity of these complexes.

RMSF analysis of β-lactamase protein dynamics in ligand-bound simulations

The reliability of each amino acid residues of the β-lactamase of *A. baumannii* dynamic behavior for 100 ns of molecular dynamics simulation in the presence of α-Terpinen-7-al and γ-Terpinen-7-al were analyzed using Root Mean Square Fluctuation (RMSF) method. The RMSF is a measure of the deviation of each residue to an average position during the simulation. This is a direct measure of the local flexibility. The RMSF plots for (Panel A: α-Terpinen-7-al; Panel B: γ-Terpinen-7-al) show that most of the residues have lower RMSF values. This value corresponds to a stable protein backbone as well as a low atomic mobility. However, the highest RMSF peaks (to

Compound	HOMO (eV)	LUMO (eV)	Energy gap (eV)
α-Terpinen-7-al	0.021922	0.06463	0.42708
γ-Terpinen-7-al	0.020062	0.06145	0.41076

Table 11. Comparison of HOMO, LUMO energy level, and energy gap (ΔE) for α-Terpinen-7-al, γ-Terpinen-7-al.

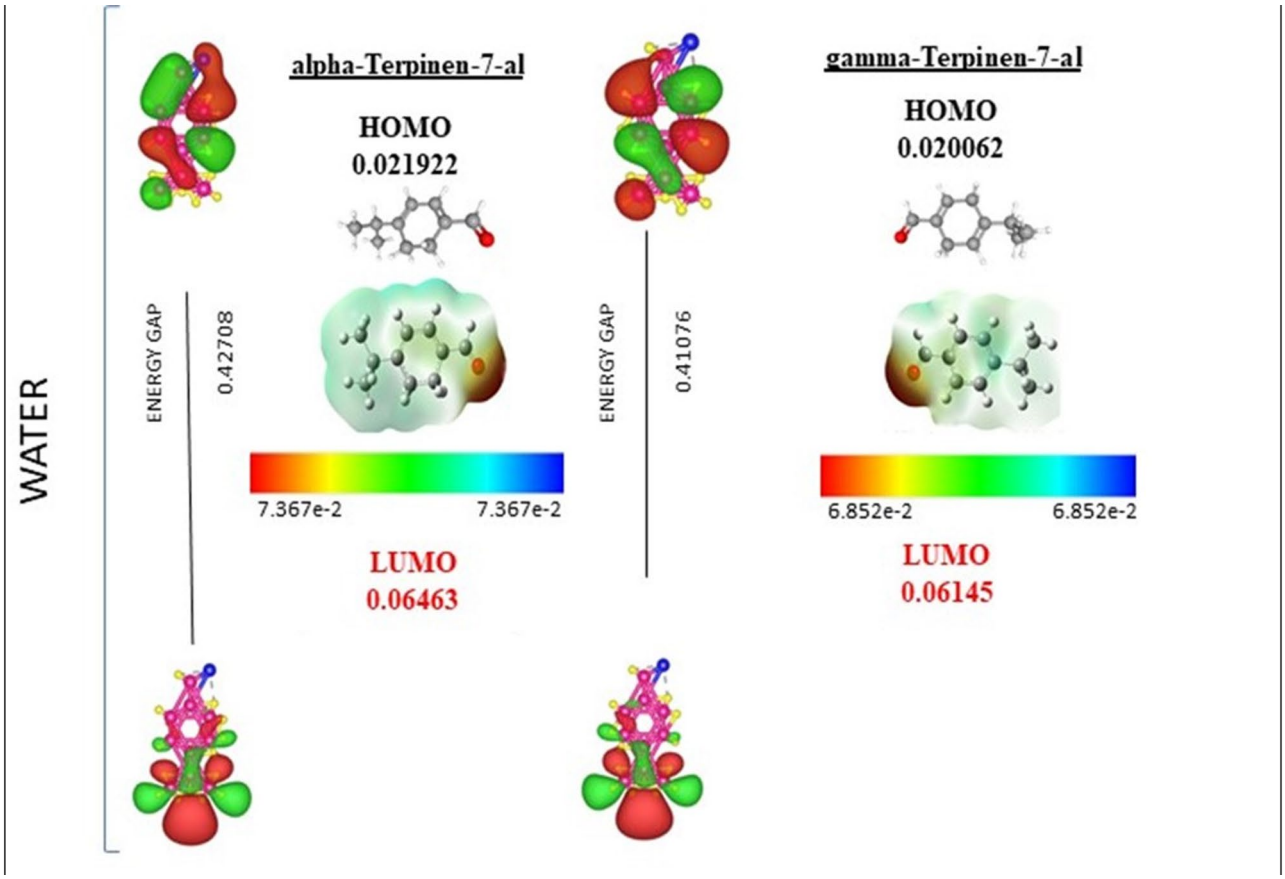

Fig. 5. Electronic properties of α-Terpinen-7-al (left panel) and γ-Terpinen-7-al (right panel) showing HOMO/LUMO distributions, energy gaps, and molecular electrostatic potential (MEP) maps (FMOs and MESP visualized on VESTA Version 3 and Gauss view software 6.0 respectively).

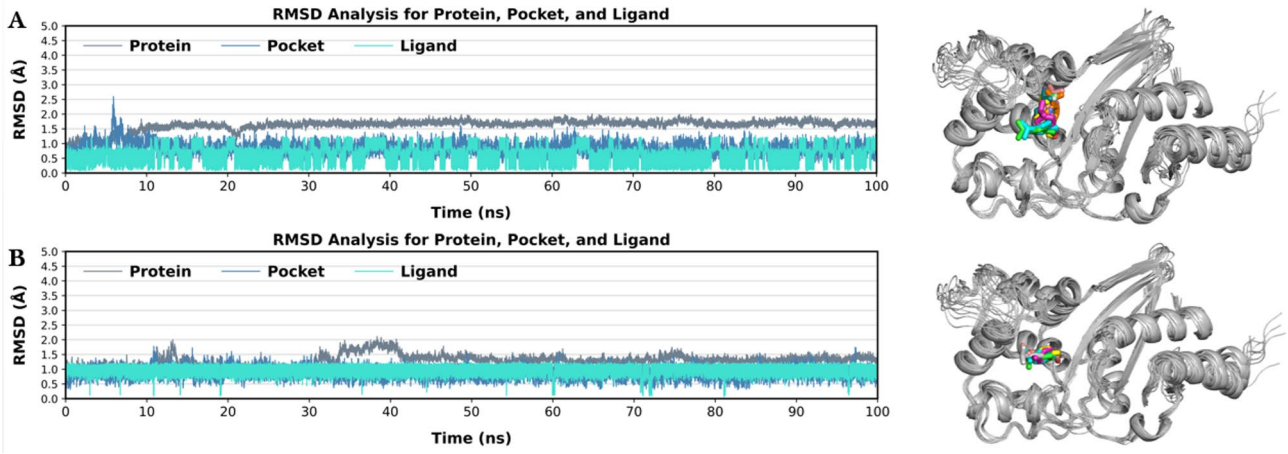

Fig. 6. RMSD analysis of *A. baumannii* protein-ligand complexes after 100 ns MD simulation, showing deviations in the structure of the protein, binding pocket, and ligand. Structural models show the binding of the ligand in the active site of the protein (Generated using AmberTools20).

~ 1.5 to 2.5 Å) arise in the N- and C-termini and in several loop regions. These regions tend to be more flexible because they have less secondary structure and greater solvent accessibility. Lower RMSF values were observed in the core secondary structure elements (α-helix and β-sheet), indicating their rigidity and structural stability. Moderate fluctuations were observed in residues located near the active-site region, suggesting that ligand binding induces localized flexibility within the binding pocket. These fluctuations likely reflect conformational

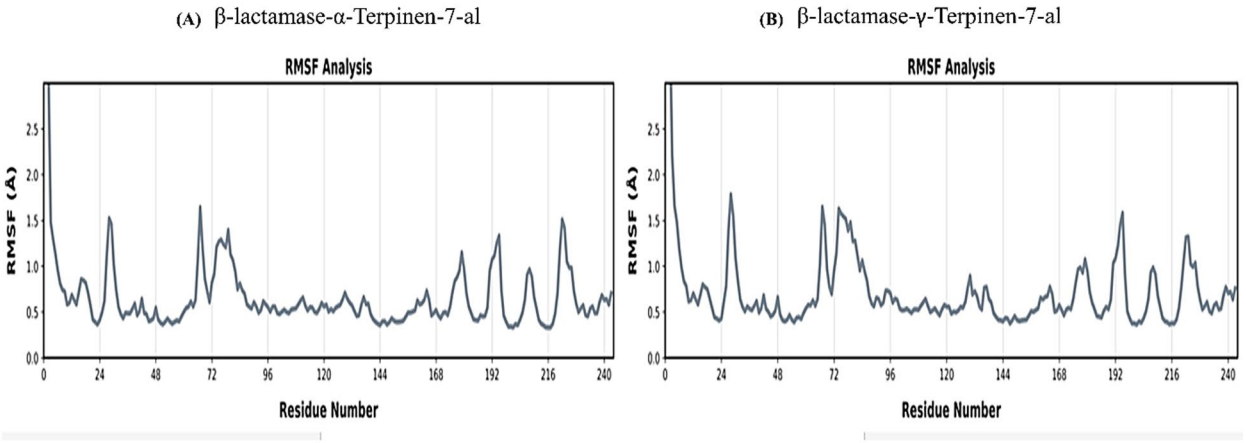

Fig. 7. RMSF profiles of β-lactamase from *A. baumannii* in complex with (**A**) α-Terpinen-7-al and (**B**) γ-Terpinen-7-al, as determined by 100 ns molecular dynamics simulations (Generated using AmberTools20).

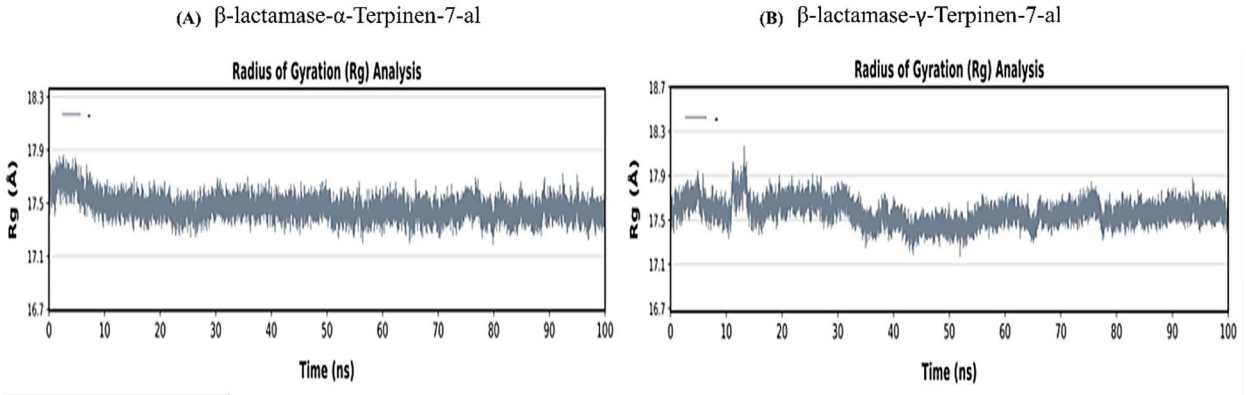

Fig. 8. Radius of gyration (Rg) profiles of β-lactamase from *A. baumannii* in complex with (**A**) α-Terpinen-7-al and (**B**) γ-Terpinen-7-al during 100 ns molecular dynamics simulations (Generated using AmberTools20).

adjustments required to accommodate the ligand, while the overall structural framework of the protein remains stable. In contrast, larger fluctuations were mainly observed in loop and terminal regions, which are generally more flexible. The RMSF profiles suggest similar conformational stability of the β-lactamase complexed with α-Terpinen-7-al and γ-Terpinen-7-al. Expected flexibility was observed only in the peripheral regions, whereas the active site remained structurally stable throughout the simulation (Fig. 7).

Radius of gyration (Rg) analysis of B-lactamase complexes with α- and γ-Terpinen-7-al

The radius of gyration (Rg) was employed to assess the compactness and stability of the movement of β-lactamase from *A. baumannii* over 100 ns molecular dynamics simulations with α-Terpinen-7-al and γ-Terpinen-7-al. Rg is the root mean square distance of the atoms in a protein from its center of mass and serves as a key representation of the spatial distribution and compactness of the protein.

For the complex of β-lactamase with α-Terpinen-7-al (Panel A of Fig. 8), the Rg values went from about 17.3 to 17.9 Å during the simulation. Likewise, the Rg values of the complex of the enzyme β-lactamase and γ-Terpinen-7-al (Panel B of Fig. 8) have been in the interval ~ 17.4–18.3 Å. Both the complexes exhibited relatively stable Rg profiles with slight fluctuations and remained relatively compact in the 100 ns extended simulation. In conclusion the stable Rg profiles of both complexes reveal that the binding of the ligand maintains the compactness and stability of the β-lactamase during the simulation which is consistent with the protein complexes having their structural stability intact. This suggests that α-Terpinen-7-al and γ-Terpinen-7-al stably interact with the active sites of β-lactamase without disrupting its global fold, thereby supporting their potential activity as effective antimicrobial complexes under simulated conditions.

Solvent accessible surface area (SASA) analysis of B-lactamase complexes α-Terpinen-7-al and γ-Terpinen-7-al during molecular dynamics simulation

A very important component, the Solvent Accessible Surface Area (SASA), which quantifies solvent exposure on a protein surface, was studied for the β-lactamase complex with α-Terpinen-7-al and γ-Terpinen-7-al in the

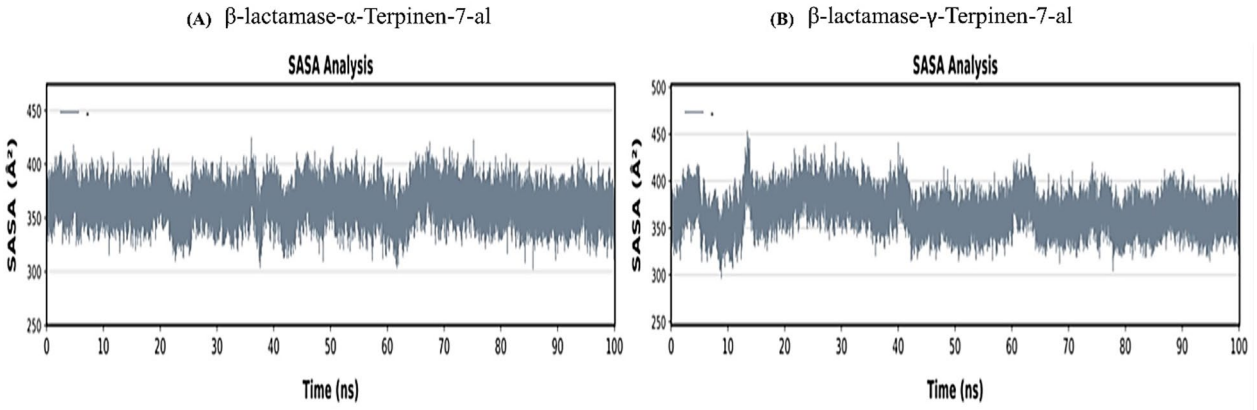

Fig. 9. Solvent Accessible Surface Area (SASA) Analysis of β-lactamase Complexes with α- and γ-Terpinen-7-al during 100 ns Molecular Dynamics Simulation. (**A**) SASA profile of the β-lactamase-α-Terpinen-7-al complex from *A. baumannii*. (**B**) SASA profile of the β-lactamase-γ-Terpinen-7-al complex from *A. baumannii* (Generated using AmberTools20).

Energy component (kcal/mol)	α-Terpinen-7-al-β-lactamase	γ-Terpinen-7-al-β-lactamase
Gas Phase Energy (ΔG < sub> gas</sub>)		
van der Waals (ΔE < sub> vdW</sub>)	−31.7996	−23.826
Electrostatic (ΔE < sub> ele</sub>)	−12.7364	−11.525
Total Gas Phase Energy	−31.536	−30.351
Solvation Free Energy (ΔG < sub> sol</sub>)		
Polar Contribution (ΔG < sub> ele</sub>)		
GB Model	17.6492	15.3953
vPB Model	26.0251	23.8991
Nonpolar Contribution (ΔG < sub> nonpol</sub>)	−5.8685	−3.4607
Total Solvation Energy	11.6492	11.9347
Final Predicted Binding Free Energy (ΔG < sub> pred</sub>)		
GB Model (ΔG < sub> pred, GB</sub>)	−37.8869	−23.416
PB Model (ΔG < sub> pred, PB</sub>)	−15.3705	−12.121

Table 12. The table organizes the binding free energy components calculated using the MM/GBSA and MM/PBSA methods for the interaction between Terpinen-7-al Isomers and *A. baumannii*β-lactamase.

current study. SASA for the *A. baumannii* β-lactamase-α-Terpinen-7-al complex during a 100 ns molecular dynamics simulation, showing solvent exposure of the protein. The solution net area (SASA values) oscillated in the range of 320–420 Å², indicating the presence of a certain solvent over time, which is supported by minor variations showing a uniform exposition of the protein surface to the solvent (Plot A of Fig. 9). Plot B of Fig. 9 shows the SASA for *A. baumannii* under another simulation condition (following a solvated ligand that measures β-lactamase-γ-Terpinen-7-al complex solvent exposure). In this case, the SASA values ranged from 300 to 450 Å². The rapid initial increase in SASA observed during the early 10–20 ns could indicate partial protein unfolding, which may lead to recovery and stabilization through solvent interactions. This indicates that the protein achieved and maintained a conformational equilibrium for the remainder of the simulation. This finding also maintains a modest opening during the initial phase, with subsequent reinforcement and size maintenance upon reaching equilibrium. These results are consistent with the known dynamics of solvent-interaction-driven protein unfolding and refolding.

Calculation of binding free energy (MM/PBSA)

The Molecular Mechanics/Poisson-Boltzmann Surface Area (MM/PBSA) method was used to calculate the binding free energies of α-Terpinen-7-al and γ-Terpinen-7-al inhibitors against *A. baumannii* β-lactamase in this study, using 1000 snapshots of 20 ns simulations. The computations were performed using MM/PBSA. It was created as an MPI1 package, and binding affinities were compared with the bacterial protein structure using these two ligands. The predicted binding free energies (ΔGpred) based on the Generalized Born (GB) method showed that α-Terpinen-7-al had the strongest binding affinity with a score of −37.8869 kcal/mol, followed by γ-Terpinen-7-al, which exhibited a slightly weaker affinity (−23.4158 kcal/mol) (Table 12). This shows that α-Terpinen-7-al binds more strongly to the β-lactamase protein than γ-Terpinen-7-al, which agrees with the experimental affinities for both the loosely bound H and the tightly bound L. The improved binding

of α-Terpinen-7-al may be due to important interactions such as SER-83, GLY-101, GLU-103, ALA-103, LEU-104, ALA-105, and THR-148. These residues serve to stabilize the ligand in the binding pocket. They may do so directly by increasing the affinity or constraining the conformational flexibility of the residues comprising the inhibitor-binding pocket. The electrostatic interactions (ΔEele) in both vacuum and solvent for α-Terpinen-7-al (−2.7364 kcal/mol) were quite similar to those of γ-Terpinen-7-al (−11.5248 kcal/mol). The electrostatic solvation penalties, as manifested in ΔGpolar (PB) (26.0251 kcal/mol for α-Terpinen-7-al and 23.8991 kcal/mol for γ-Terpinen-7-al), however, penalize ligand binding because the desolvation penalty opposes the favorable Coulomb interactions between the ligands and the protein. This was also supported by the solvation-free energies (ΔGsol) of 11.6492 kcal/mol for α-Terpinen-7-al and γ-Terpinen-7-al, which reveal the desolvation contribution to the binding process. Conversely, based on the MM-GBSA results, the van der Waals (ΔEvdW) forces and nonpolar solvation energies (ΔGnonpol) were significant energy components for all ligands. For van der Waals interaction, α-Terpinen-7-al showed the lowest energy (−32.7996 kcal/mol), whereas γ-Terpinen-7-al was the second one with − 28.8257 kcal/mol. Likewise, in the presence of nonpolar solvation, ΔGnonpol, the overall contribution (ΔEvdW + ΔGnonpol) indicates that α-Terpinen-7-al is a stronger binder. The results suggested that hydrophobic interactions and non-covalent bonds play a key role in preserving ligands inside the binding pocket. The sum of ΔEele + ΔGele + ΔGsol (electronic and solvation energy contributions) was also computed. The α-Terpinen-7-al was bound better with a ΔEele + ΔGele + ΔGsol (GB) of 4.9128 kcal/mol versus γ-Terpinen-7-al, at 3.8705 kcal/mol. Moreover, the MMPBSA analysis of *A. baumannii* β-lactamase revealed that van der Waals and nonpolar solvation energies are major contributors to the higher binding affinity of α-Terpinen-7-al compared with γ-Terpinen-7-al. Electrostatic interactions are not negligible, but they can be unfavorable in many cases, and desolvation effects can completely cancel out the otherwise stabilizing effects of either type of electrostatic interaction. The high affinity of α-Terpinen-7-al may result from its engagement with critical residues, suggesting possible opportunities for optimization and future validation as an antibacterial agent.

Discussion

The emergence of multidrug-resistant (MDR) microorganisms is a major global health burden[42]. *A. baumannii*, one of the critical WHO pathogens, possesses outstanding drug resistance mechanisms, such as efflux pump overexpression, degradation of antibiotics by enzymes, and the ability to form a biofilm, resulting in nosocomial pneumonia, bloodstream, and wound infections with 40–70% mortality among immunocompromised patients[43]. The glycocalyx of the emerging tide of XDR and PDR strains has made conventional antibiotics increasingly ineffective, calling for other treatment options[44]. Plant-derived phytochemicals, which compose 30–50% of the available drugs, are promising sources of safe and stable antimicrobial agents against resistant pathogens[45]. The ethanolic extract of *A. foemina* shows potent antimicrobial activity on extensively drug-resistant *A. baumannii* isolates using an in-depth analysis combining profiling of phytochemicals, biochemical characterization and computational validation. This investigation reveals that the chemically complex composition of the extract with distinct implications for the observed antimicrobial efficacy can only be interpreted in a systematic way in multiple biological and computational frameworks. Detailed GC–MS profiling of the *A. foemina* ethanol extract revealed the presence of 16 bioactive phytocompounds. The extract displays a rather interesting compositional bipartition with a predominance of a lipophilic fraction represented by polyunsaturated fatty acids and their ester derivatives (56% combined relative abundance) accompanied by minor yet bioactive monoterpene aldehydes (α-Terpinen-7-al and γ-Terpinen-7-al, respectively, at 1.62% and 1.70%). The rational prioritization of these, based on the documented efficacy of monoterpenes against resistant Gram-negative bacteria, is justified by these computations[46]. The chemical diversity (e.g., terpenoids, fatty acids, phytosterols, and vitamins) supports multifactorial antimicrobial mechanisms, unlike conventional β-lactams. Unsaturated fatty acids (18.48% in total) have known antibacterial features through membrane disruption and lipid peroxidation[47].

Agar well diffusion assays showed inhibition zones of 20.16 ± 0.29 mm at an extract concentration of 15 mg/mL, which is 2.5 times greater than the imipenem-positive control (8 mm at 10 µg). However, proper interpretation of this comparative efficacy requires standardization on an active compound basis. In this extract, the content of α-Terpinen-7-al is only 1.62%, resulting in a much lower mole concentration of the actual aldehyde than the total extract concentration. Direct efficacy comparisons on an individual phytocompound basis require isolation and independent testing of the individual compounds, prerequisites for evaluating inhibitory mechanisms. The minimum inhibitory concentration of 1.25 mg/mL, combined with the minimum bactericidal concentration of 2.5 mg/mL, yielded a minimum bactericidal concentration to minimum inhibitory concentration ratio of 2.0, which is well above the threshold for bacteriostatic activity of 4.0, indicating potent bactericidal activity. The narrow window of concentration required to distinguish between growth inhibition and 99.9% bacterial killing suggests engagement of specific antimicrobial mechanisms rather than non-selective cytotoxicity. Of note, the observed bactericidal efficacy was similar across all three tested isolates despite potential phenotypic and genotypic heterogeneity, suggesting strain-independent mechanisms; however, broader evaluation across diverse geographic regions and carbapenemase genotypes would be required to establish generalized claims[48]. The polyunsaturated fatty acid components, although showing considerable relative abundance and documented antimicrobial properties in the literature, are likely to act through mechanisms very different from direct enzyme inhibition. These compounds, such as linoleic acid and α-linolenic acid, are antimicrobial because they promote lipid peroxidation by producing reactive oxygen species and perturbing the membrane phospholipid bilayer[49]. Molecular docking analysis supported this mechanistic difference, showing that fatty acid components exhibited weak docking affinities (range of −1.9 to −2.7 kcal/mol), poor geometric accommodation within the OXA-24 active site-tunnel, and a lack of predicted hydrogen bonds with catalytic residues (Supplementary Table S3). The minor monoterpene aldehydes, on the contrary, despite representing < 2% of the total extract area, showed considerably better predicted binding affinities and residue engagement in the catalytic reaction. This structure-function discordance exemplifies how abundance-based compound prioritization can mask bioactive

potential in complex plant extracts. The antimicrobial efficacy of the whole extract is likely due to the combined action of multiple mechanisms rather than the contribution of individual compounds. Fatty acid components may enhance the penetration of aldehyde compounds by destabilizing membranes, modify the function of efflux pumps through lipid modification, or exert a general antimicrobial effect on phenotypically distinct subpopulations of the bacterial population[50]. This hypothesis of a dual-mechanism antimicrobial phenotype is supported by an MBC/MIC ratio of 2.0, indicating the involvement of multiple inhibitory pathways.

Molecular docking analysis showed fundamentally distinct binding affinities of 16 identified compounds to OXA-24 β-lactamase. Only two compounds reached predicted binding free energies in the moderate affinity classification (ΔG −5.0 to −8.0 kcal/mol), α-Terpinen-7-al (−5.4 kcal/mol, highest affinity compound) and γ-Terpinen-7-al (−5.3 kcal/mol, second highest affinity compound). Both isomers are monocyclic monoterpenes with an aldehyde functional group at the C7 position, which is absent in the 14 non-selected compounds[51]. The remaining compounds showed weak to very weak predicted affinities (ΔG = −1.5 to −3.8 kcal/mol), providing computational justification for selectively prioritizing further investigation of compounds containing aldehyde groups. Detailed analysis of predicted binding modes showed convergent binding: both isomers interact with the catalytic residue Ser-81 by forming important hydrogen bonds at a structurally equivalent position to the canonical catalytic serine of OXA-24. Predicted hydrogen bond distances (about 3.1 Å) for both isomers with Ser-81 are compatible with a functional hydrogen-bonding geometry. Additional stabilization comes from nonpolar interactions between the hydrophobic residues Tyr-112 and Val-130, which bury the cyclic ring system in the substrate-binding pocket. The predictive geometry places the aldehyde carbonyl oxygen toward the catalytic serine, and, because of the conformational preorganization in the cyclic structure, there is a possibility of mechanism-based inhibition through the formation of a Schiff base (imine linkage between the aldehyde carbon and the serine hydroxyl nucleophile). If formed under physiological conditions, such an aldimine intermediate would be theoretically stable to hydrolysis, potentially rendering the catalytic serine unable to regenerate its nucleophilic hydroxyl group[52]. However, this proposed mechanism is still computational prediction; experimental validation through pre-steady state kinetic analysis and mass spectrometry detection of the enzyme-compound covalent adducts and hydroxylamine reactivity rescue assays would be required to confirm mechanism-based inactivation. The predicted mechanism differs from irreversible inhibition by penam sulfone inhibitors (such as SA-1-204), which are reported to induce irreversible decarboxylation of Lys-84 in OXA-24 enzymes[53]. Instead, the mechanism would involve imine formation with Ser-81 (targeting the catalytic serine) rather than with Lys-84 (targeting the auxiliary lysine residue). This mechanistic distinction may have pharmacological importance since compounds that are refractory to bicarbonate-mediated reactivation (as is characteristic of classical serine β-lactamase inhibitors) may be resistant to bacterial resistance mechanisms that have developed to counteract current marketed inhibitors[54].

Molecular dynamics simulations lasting 100 nanoseconds were performed to assess the dynamic stability of the predicted docking poses. The value of root mean square deviation (RMSD) for the complex between α-Terpinen-7-al-OXA-24 was stable all along the simulation trajectory, with a mean value of 1.5 ± 0.3 Å, indicating that the α-Terpinen-7-al-OXA-24 complex occupies the predicted binding pocket continuously, without significant conformational drift or dissociation of the ligand. In contrast, the RMSD fluctuations of the model in the γ-Terpinen-7-al complex were (mean 1.0 ± 0.3 Å) . These molecular dynamics results show that the computed binding geometries are thermodynamically and kinetically stable under simulated physiological conditions, a prerequisite of putative mechanism-based inhibition. Root-mean-square fluctuation analysis showed anticipated flexibility in the terminal and loop regions without compromising the structural integrity of the active site. The radius of gyration was constant throughout both simulations (17.3–18.1 Å) and confirmed the absence of deleterious global protein unfolding with the binding of the ligand. Solvent-accessible surface area profiles showed minor fluctuations, consistent with equilibration dynamics and stable protein-ligand complexes formation. These molecular dynamics results support the computational feasibility of the predicted mechanisms, but do not provide evidence of functional inhibition without biochemical validation through enzyme kinetics.

Binding free energy calculations by using molecular mechanics/Poisson-Boltzmann surface area (MM/PBSA) methodology have predicted substantially different binding energies from the docking scores of results of AutoDock Vina: α-Terpinen-7-al yielded a binding free energy of −37.9 kcal/mol, and γ-Terpinen-7-al exceeded the value of −23.4 kcal/mol. This difference between docking scores (AutoDock: −5.4 and − 5.3 kcal/mol) and MM/PBSA estimates is likely due to differences in scoring function methodology, as AutoDock Vina is an empirical scoring function parameterized for drug-like molecules, and MM/PBSA is a much more computationally expensive energy decomposition including solvation effects and entropic contributions. The MM/PBSA estimates, while theoretically more rigorous, may overestimate binding affinity for small natural product scaffolds due to limitations in the GB solvation model and the lack of entropy contributions[55]. Residue-by-residue energy decomposition results showed that van der Waals interactions (ΔE_vdW: −31.8 kcal/mol in the case of α-isomer) and nonpolar solvation contributions (ΔG_nonpol) predominate the binding thermodynamics, and it demonstrated hydrophobic effect-driven binding. Electrostatic contributions, although large in isolation (ΔE_elec: −2.7364 to −12.7364 kcal/mol), are significantly reduced by the polar solvation penalties (ΔG_GB or ΔG_PB; +26.0 kcal/mol for α-isomer), in accordance with the desolvation penalty associated with the relocation of a polar hydrogen bond from the water phase to the protein interior. These energetic decompositions yield mechanistic insight into the binding-driving forces, but need to be validated experimentally using calorimetric approaches to obtain absolute binding free energies[56].

Density functional theory calculations provided quantum-chemical insight into electronic properties, yielding predictions of reactivity. HOMO-LUMO energy gap calculations for the substrates, α-Terpinen-7-al and γ-Terpinen-7-al, yielded values of 0.427 eV and 0.411 eV, respectively, indicating relatively low energy requirements for electronic transitions. The existence of such small energy gaps, within a range reported for known antimicrobial compounds, therefore implies favorable electronic properties for nucleophilic attack by

catalytic residues. Molecular electrostatic potential surface analysis revealed an increase in electron density at the carbonyl carbon and the adjacent unsaturated ring, consistent with electrophilic carbonyl character and the susceptibility to nucleophilic addition by protein nucleophiles (serine hydroxyl oxygen or activated nucleophiles)[57]. Due to the similarity of electronic characteristics between the α- and γ-isomers, despite their differentiated docking affinities, reactivity differences are primarily driven by geometric fit within the active site (shape complementarity) rather than by electronic properties. These insights from computational chemistry support docking predictions and provide further theoretical support for the feasibility of aldehyde lysine/serine condensation reactions, though DFT calculations alone cannot predict biological reactivity without considering protein microenvironment and entropy effects[58]. The pronounced biofilm inhibition of *A. foemina* extract at sub-MIC concentrations (86.57 ± 6.40% inhibition at MIC; 32.84 ± 2.42% at 0.078 mg/mL) suggests mechanistic selectivity for biofilm disruption compared with conventional antimicrobials. The fact that biofilm inhibition exceeds growth inhibition at concentrations below the biofilm growth inhibitory concentration may indicate mechanistic selectivity: the extract may preferentially target the biofilm structure, adhesin expression, or quorum-sensing regulatory circuits at concentrations too low to kill planktonic cells. *A. baumannii* biofilm formation is regulated by complex networks that control adhesin protein synthesis, exopolysaccharide biosynthesis, and quorum-sensing-mediated phenotypic switching[59]. Anti-quorum-sensing and anti-adhesion effects of terpenoids and polyunsaturated fatty acids structurally related to *constituents of A. foemina* have been documented in the literature[60]. Monoterpene aldehydes and related oxygenated terpenes inhibit biofilm formation by interacting with the EPS biosynthetic machinery and cross-linking enzymes[61]. Phytol (8.81% found in extract) is reported to inhibit type I pili and pap adhesins that are critical to *A. baumannii* attachment to abiotic and biotic surfaces[62]. However, these proposed mechanisms remain speculative, lacking dedicated experimental validation: the present study provides evidence of an observable biofilm inhibition phenotype but offers no details on which compound(s) mediate this effect or through which specific regulatory pathway(s). Future research using biofilm-deficient mutants, quorum-sensing reporter strains, and directed transcriptomic analysis would be needed to establish the mechanism of action for the observed anti-biofilm activity.

In silico ADMET analysis predicted that the prioritized compounds had favorable drug-like properties. Both α-Terpinen-7-al and γ-Terpinen-7-al meet Lipinski's Rule of Five (molecular weight < 500 g/mol, HBA < 10, HBD < 5, reasonable oral bioavailability potential). LogP values of 2.26 and 2.10, respectively, are, however, within the optimal range (1–3) for antimicrobial agents and sufficient for membrane penetration, while avoiding excessive protein binding. Predicted gastrointestinal absorption was greater than 80%, suggesting possible oral therapeutic administration. Significantly, both compounds are predicted not to be substrates for the P-gp efflux transporter, thereby reducing the likelihood of expulsion from cells and potentially enhancing intracellular accumulation. Blood-brain barrier penetration is predicted to be positive for both isomers, though clinical significance for CNS infections remains to be evaluated. However, these predictions are computational estimates based on statistical models trained on chemical databases; they are not experimental demonstrations of bioavailability, distribution, or tissue penetration. Systematic evaluation of predicted properties requires experimental validation using *in vitro* absorption assays (intestinal epithelial transport using Caco-2 or similar models), plasma protein binding determination, microsomal stability, and *in vivo* pharmacokinetic assays in appropriate animal models before evaluating translational feasibility[63]. The predicted stability in metabolism (no inhibition of CYP450 enzymes) and a favorable toxicity profile (no signals of toxicity in Ames test, Hepatotoxicity, Cardiotoxicity) are strong arguments for proceeding to preclinical evaluation; however, *in vitro* toxicological characterization (cell viability assay, genotoxicity test by comet assay) is recommended. *In vivo* safety evaluation by animal infection models would be a prerequisite for clinical translation[64]. The results of this study show that *A. foemina* phytocompounds are lead identification-stage candidates for antimicrobial drug discovery instead of validated drug candidates. The multimodal analysis combining phytochemistry, biochemical antimicrobial analysis, molecular docking, molecular dynamics validation, electronic property analysis by DFT, ADMET prediction, and biofilm inhibition profiling provides a comprehensive set of tools that offers full ex vivo/ex in silico support for the antimicrobial hypothesis. The overlap of information from multiple analytical modes provides greater confidence: biochemical observations (MBC/MIC = 2.0, biofilm inhibition > 86%) support a favorable binding affinity and stable complex dynamics in computer simulations.

However, the significant gaps between computational prediction and functional validation, most importantly the lack of direct enzymatic inhibition kinetics, confirmation of mechanism-of-action, etc., necessarily limit conclusions relating to absolute inhibitory potency or clinical translational potential at this stage of investigation. This study reveals interesting scaffolds of natural products that warrant mechanistic investigation; efficacy as validated therapeutics remains to be established.

The importance of this investigation extends to the broader problem of antimicrobial resistance: *A. baumannii* is listed by the World Health Organization as a critical-priority pathogen linked to roughly 57,000 deaths per year, and > 74% of global clinical isolates are carbapenem-resistant. The erosion of antimicrobial options with efficacy, especially against extensively drug-resistant and pan-drug-resistant phenotypes, requires the investigation of novel inhibitor scaffolds[65]. Current clinical β-lactamase inhibitors include clavulanic acid, sulbactam, and tazobactam, and are all based on semi-synthetic modifications of the β-lactam ring and not fundamentally different chemical scaffolds. Natural products are a vast, uncharted resource of bioactive lead compounds for scaffold-based drug discovery. The Terpinen-7-al-based mechanism, if experimentally proven, would represent a new mechanism of inhibition, distinct from both irreversible serine β-lactamase inhibition and the classical Lys-84 decarboxylation resistance mechanisms. Such a mechanistic novelty may confer resistance-evasion potential, enabling therapeutic efficacy against clinical isolates refractory to existing inhibitor classes.

Several limitations need to be explicitly recognized. First, molecular docking and dynamics simulations yield structural and energetic predictions but do not constitute functional evidence of enzyme inhibition. Establishment of the proposed mechanism includes: (1) pre-steady-state kinetic analysis by stopped-flow

spectrophotometry or isothermal titration calorimetry experiments for the detection of transient enzyme intermediates; (2) the confirmation of covalent enzyme-compound intermediates by mass spectrometry analysis; and (3) hydroxylamine rescue assays for the determination of reversibility of the putative Schiff base intermediate. Second, the current study tested only three clinical *A. baumannii* isolates; testing representative diversity of strains from different geographic regions, different collection time periods, and different carbapenemase genotypes would be necessary to make generalized claims of efficacy. Third, the investigation was limited to the role of OXA-24 β-lactamase as a target of resistance; *A. baumannii* multifactorial resistance additionally involves efflux pump overexpression (AdeABC, AbeM), outer membrane porin downregulation, and ribosomal target modification. The research did not address whether *A. foemina* compounds interact with these non-enzymatic forms of resistance, nor did it evaluate combinatorial efficacy in intact bacteria versus isolated enzyme systems. Fourth, the data are all based upon *in vitro* assays; pharmacokinetic behavior, tissue penetration, toxicological, or therapeutic efficacy in animal models of infection remain unexplored. Fifth, the botanical extract composition has intrinsic variability dependent on the plant part collected, seasonally relevant factors, growing conditions, and the extraction procedure. Standards for bioactive compound concentrations and for evaluating phytochemical stability during storage and processing are prerequisites for translational development.

Conclusion

This integrated biochemical and computational investigation demonstrates that *A. foemina* Mill. The extract exhibits potent antimicrobial activity against extensively drug-resistant *A. baumannii* isolates. GC- MS revealed 16 constituents with a bipartite structure in which polyunsaturated fatty acids are predominant (56%), whereas minor monoterpene aldehydes (α-Terpinen-7-al 1.62%, γ-Terpinen-7-al 1.70%) exhibit an enhanced predicted binding to OXA-24 β-lactamase through molecular docking and molecular dynamics simulations. The antimicrobial activity is probably mediated, in part, through these minor constituents, but the extent to which they contribute to antimicrobial activity needs to be biochemically validated. Bactericidal activity is confirmed by several quantitative tests, as follows: MBC/MIC ratio of 2.0; agar well diffusion zones of 20.16 ± 0.29 mm (20 mg/mL) vs. 8 mm for imipenem (2.5 times); and biofilm inhibition > 86% at the MIC. These results are consistent with several possible mechanisms: the putative inhibition of OXA-24 that was predicted for monoterpene aldehydes (needs validation by enzyme kinetics), and possible membrane effects predicted for polyunsaturated fatty acids (mechanism to be elucidated). The differential biofilm inhibition at sub-MIC concentrations is indicative of selective anti-biofilm activity and may be due to quorum-sensing inhibition and/or adhesin disruption, but this needs to be validated experimentally. Computational analysis, including molecular docking (GlideScore: −5.4 kcal/mol for α-Terpinen-7-al, −5.3 kcal/mol for γ-Terpinen-7-al), molecular dynamics simulation (100 ns, RMSD < 2.5 Å), free energy of binding, DFT analysis, and ADMET prediction, is consistent with the observed antimicrobial phenotype. However, these analyses provide only a theoretical rationale and do not constitute experimental validation of the mechanism or efficacy. These findings provide a foundation for investigating *A. foemina*-derived terpenoids as antimicrobial lead candidates. Introducing plant-derived therapeutics to the clinical level requires many steps: the detailed characterization of enzyme kinetics, including pre-steady state analysis, for purified compounds; evaluation of the resistance towards non-enzymatic mechanisms of resistance such as efflux pumps and permeability; investigation of the mechanisms of biofilm formation using mutant panels and transcriptomic profiling; pharmacokinetic evaluation in small animal models, *in vivo* evaluation of efficacy and safety and botanical standardization. These plant-based scaffolds are particularly relevant in light of the major threat of carbapenem resistant strains of *A. baumannii* (a priority microorganism as identified by the WHO). However, bringing these compounds to the clinic requires a long preclinical and clinical development process and regulatory approval as well as large-scale production. Such comprehensive efforts are one way to give such efforts a mechanistic basis.

Data availability

The analyzed dataset of this study is included in the manuscript. The datasets produced and/or analyzed during the current research are available at the DNA Data Bank of Japan (DDBJ) repository under the Accession Numbers of LC905275, LC905276 and LC905277. Other datasets (GC–MS) are available at https://doi.org/10.5281/zenodo.17760388.

Received: 20 November 2025; Accepted: 16 March 2026
Published online: 30 March 2026

References

1. Roque-Borda, C. A. et al. Challenge in the discovery of new drugs: Antimicrobial peptides against WHO-list of critical and high-priority bacteria. *Pharmaceutics* **13**, 773. https://doi.org/10.3390/pharmaceutics13060773 (2021).
2. Kostrzewa, M., Nagy, E., Schröttner, P. & Pranada, A. B. How MALDI-TOF mass spectrometry can aid the diagnosis of hard-to-identify pathogenic bacteria–the rare and the unknown. *Expert Rev. Mol. Diagn.* **19**, 13238. https://doi.org/10.1080/14737159.2019.1643238 (2019).
3. Abdul-Mutakabbir, J. C., Griffith, N. C., Shields, R. K., Tverdek, F. P. & Escobar, Z. K. Contemporary perspective on the treatment of *Acinetobacter baumannii* infections: Insights from the Society of Infectious Diseases Pharmacists. *Infect. Dis. Ther.* **10**, 2177–2202. https://doi.org/10.1007/s40121-021-00541-4 (2021).
4. Alrahmany, D., Omar, A. F., Alreesi, A., Harb, G. & Ghazi, I. M. *Acinetobacter baumannii* infection-related mortality in hospitalized patients: Risk factors and potential targets for clinical and antimicrobial stewardship interventions. *Antibiotics* **11**, 1086–1096. https://doi.org/10.3390/antibiotics11081086 (2022).
5. Gheorghe, I. et al. Subtypes, resistance and virulence platforms in extended-drug resistant *Acinetobacter baumannii* Romanian isolates. *Sci. Rep.* **11**, 13288. https://doi.org/10.1038/s41598-021-92590-5 (2021).

6. Douzandeh-Mobarrez, B., Alizade, H., Kafil, H. S. & Karmostaji, A. Antimicrobial categories in describing multidrug resistance, extensive drug resistance and pan-drug resistance in *Pseudomonas aeruginosa* and *Acinetobacter baumannii*: a systematic review. *RRMM* **32**, 6–11. https://doi.org/10.1097/MRM.0000000000000235 (2021).
7. Sobouti, B. et al. Pan drug-resistant *Acinetobacter baumannii* causing nosocomial infections among burnt children. *Med. J. Islam Repub. Iran.* **34**, 24. https://doi.org/10.34171/mjiri.34.24 (2020).
8. Shadifar, H. et al. Antibacterial and synergistic effects of aqueous and methanol extracts of artemisia annua against multidrug-resistant isolates of *acinetobacter*. *Anti-Infect Agents*. **19**, 28–35. https://doi.org/10.2174/2211352518999200525002520 (2021).
9. Başaran, S. N. & Öksüz, L. The role of efflux pumps in antibiotic resistance of gram negative rods. *Arch. Microbiol.* **205**, 192. https://doi.org/10.1007/s00203-023-03539-3 (2023).
10. Uddin, T. M. et al. Antibiotic resistance in microbes: History, mechanisms, therapeutic strategies and future prospects. *J. Infect. Public. Health*. **14**, 1750–1766. https://doi.org/10.1016/j.jiph.2021.10.020 (2021).
11. Abushaheen, M. A. et al. Antimicrobial resistance, mechanisms and its clinical significance. *Dis. Mon*. **66**, https://doi.org/10.1016/j.disamonth.2020.100971 (2020).
12. Wei, X. et al. Supercharged precision killers: Genetically engineered biomimetic drugs of screened metalloantibiotics against *Acinetobacter baumanni*. *Sci. Adv.* **10**, adk6331. https://doi.org/10.1126/sciadv.adk6331 (2024).
13. Zhang, L. et al. Bacterial efflux pump inhibitors reduce antibiotic resistance. *Pharmaceutics* **16**, 170. https://doi.org/10.3390/ph16020170 (2024).
14. El Mokni, R. & Domina, G. Additions to terrestrial flora of Tunisia: occurrence and taxonomic notes. *Check List.* **16**, 553–561. https://doi.org/10.15560/16.3.553 (2020).
15. López, V., Jäger, A. K., Akerreta, S., Cavero, R. Y. & Calvo, M. I. Pharmacological properties of *Anagallis arvensis* L.(scarlet pimpernel) and *Anagallis foemina* Mill.(blue pimpernel) traditionally used as wound healing remedies in Navarra (Spain). *J. Ethnopharmacol.* **134**, 215–222. https://doi.org/10.1016/j.jep.2010.12.016 (2011).
16. López, V., Cavero, R. Y. & Calvo, M. I. Cytotoxic effects of *Anagallis arvensis* and *Anagallis foemina* in neuronal and colonic adenocarcinoma cell lines. *Pharmacogn J.* **5**, 2–5. https://doi.org/10.5530/pj.2013.1.2 (2013).
17. Jiménez-López, F. J., Ortiz, P. L., Talavera, M. & Arista, M. Reproductive assurance maintains red-flowered plants of *Lysimachia arvensis* in Mediterranean populations despite inbreeding depression. *Front. Plant. Sci.* **11**, 563110. https://doi.org/10.3389/fpls.2020.563110 (2020).
18. Konatam, S. & Roy, D. N. GC–MS unveils monosaccharide D-Allose in Terminalia arjuna bark extract acting against biofilm regulatory proteins (SrtA and SarA) of Staphylococcus aureus: A drug discovery approach. *Int. J. Mass. Spectrom.* **518**, 117527. https://doi.org/10.1016/j.ijms.2025.117527 (2025).
19. Roy, D. N. *Terpenoids Against Human Diseases* (CRC, 2019).
20. Majumdar, M. & Roy, D. N. *Terpenoids Against Human Diseases* 39–60 (CRC, 2019).
21. Sun, S. et al. Impact of extraction techniques on phytochemical composition and bioactivity of natural product mixtures. *Front. Pharmacol.* **16**, 1615338. https://doi.org/10.3389/fphar.2025.1615338 (2025).
22. AL-Khikani, F. H. O., Abdullah, H. Y., Karkaz, H. M. & abdulhussein, H. A. Evaluation the combination of amoxyclav with amikacin and ceftriaxone against Escherichia coli sepsis. *Microbes Infect. Dis.* **5**, 1425–1430. https://doi.org/10.21608/mid.2023.206746.1516 (2024).
23. Hossain, T. J. Methods for screening and evaluation of antimicrobial activity: A review of protocols, advantages, and limitations. *Eur. J. Microbiol. Immunol.* **14**, 97–115. https://doi.org/10.1556/1886.2024.00035 (2024).
24. Kadeřábková, N., Mahmood, A. J. S. & Mavridou, D. A. I. Antibiotic susceptibility testing using minimum inhibitory concentration (MIC) assays. *npj Antimicrob. Resist.* **2**, 37. https://doi.org/10.1038/s44259-024-00051-6 (2024).
25. Kowalska-Krochmal, B. & Dudek-Wicher, R. The Minimum inhibitory concentration of antibiotics: Methods, interpretation, clinical relevance. *Pathogens* **10**, 165. https://doi.org/10.3390/pathogens10020165 (2021).
26. Mogana, R., Adhikari, A., Tzar, M. N., Ramliza, R. & Wiart, C. Antibacterial activities of the extracts, fractions and isolated compounds from Canarium patentinervium Miq. against bacterial clinical isolates. *BMC Complement. Med. Ther.* **20**, 55. https://doi.org/10.1186/s12906-020-2837-5 (2020).
27. Andersen, J. B., Rybtke, M. & Tolker-Nielsen, T. The dynamics of biofilm development and dispersal should be taken into account when quantifying biofilm via the crystal violet microtiter plate assay. *Biofilm* **8**, 100207. https://doi.org/10.1016/j.bioflm.2024.100207 (2024).
28. Freeman, D. J., Falkiner, F. R. & Keane, C. T. New method for detecting slime production by coagulase negative staphylococci. *J. Clin. Patho*. **42**, 872–874. https://doi.org/10.1136/jcp.42.8.872 (1989).
29. Shawky, M., Kalaba, M. H. & El-Sherbiny, G. M. Tackling carbapenem-resistant Acinetobacter baumannii (CRAB) and their virulence factors using biosynthesized silver nanoparticles combined with imipenem. *Biotechnol. Notes*. **6**, 183–195. https://doi.org/10.1016/j.biotno.2025.07.002 (2025).
30. DeLano, W. L. & Pymol An open-source molecular graphics tool. *CCP4 Newsl. Protein Crystallogr.* **40**, 82–92 (2002).
31. Dey, D. & Kumar, A. Structural-based study to identify the repurposed candidates against bacterial infections. *Curr. Med. Chem.* **32**, 3693–3718. https://doi.org/10.2174/0109298673296749240207115303 (2025).
32. Manzoor, H. et al. Linalool-based silver nanoconjugates as potential therapeutics for glioblastoma: In silico and in vitro insights. *PLoS ONE*. **20**, e0325281. https://doi.org/10.1371/journal.pone.0325281 (2025).
33. Wu, F. et al. Computational approaches in preclinical studies on drug discovery and development. *Front. Chem.* **8**, 726. https://doi.org/10.3389/fchem.2020.00726 (2020).
34. Manzoor, H. et al. Computational identification and evaluation of novel PD-L1 inhibitors for cancer immunotherapy. *Sci. Rep.* **15**, 33787. https://doi.org/10.1038/s41598-025-01232-7 (2025).
35. Veiga-Matos, J., Morales, A. I., Prieto, M., Remião, F. & Silva, R. Study models of drug–drug interactions involving P-Glycoprotein: The potential benefit of p-glycoprotein modulation at the kidney and intestinal levels. *Molecules* **28**, 7532. https://doi.org/10.3390/molecules28227532 (2023).
36. Khan, M. U. et al. Molecular docking and dynamics reveal novel CDK6 inhibitors for targeted glioblastoma therapy. *Sci. Rep.* **16**, 9000, doi:10.1038/s41598-026-39629-7 (2026).
37. Shukla, R. & Tripathi, T. Molecular dynamics simulation of protein and protein–ligand complexes. *J. Comput. Aided Mol. Des.* https://doi.org/10.1007/978-981-15-6815-2_7 (2020).
38. Manzoor, H. et al. Citronellol silver nanoconjugates as a therapeutic strategy for glioblastoma through computational and experimental evaluation. *Sci. Rep.* **15**, 1–25. https://doi.org/10.1371/journal.pone.0325281 (2025).
39. Zhang, H. et al. CHARMM-GUI free energy calculator for practical ligand binding free energy simulations with AMBER. *J. Chem. Inf. Model.* **61**, 4145–4151. https://doi.org/10.1021/acs.jcim.1c00747 (2021).
40. Manzoor, H. et al. Identification and evaluation of pyrimidine based CDK6 inhibitors against glioblastoma using integrated computational approaches. *Sci. Rep.* **15**, 25387. https://doi.org/10.1038/s41598-025-10744-1 (2025).
41. Chen, J. Computational modelling of solvent effects. *Faraday Discuss.* https://doi.org/10.26190/unsworks/24437 (2022).
42. Marino, A et al. The global burden of multidrug-resistant bacteria. *Epidemiologia* **6**, 21. https://doi.org/10.3390/epidemiologia6020021 (2025)
43. Abdi, S. N. et al. Acinetobacter baumannii efflux pumps and antibiotic resistance. *Infect. Drug Resist.* **13**, 423–434. https://doi.org/10.2147/IDR.S228089 (2020).

44. Kothari, A. et al. Age of antibiotic resistance in MDR/XDR clinical pathogen of Pseudomonas aeruginosa. *Pharmaceuticals* **16**, 1230. https://doi.org/10.3390/ph16091230 (2023).
45. Vasudevan, A. et al. In silico and in vitro screening of natural compounds as broad-spectrum β-lactamase inhibitors against Acinetobacter baumannii New Delhi Metallo-β-lactamase-1 (NDM-1). *Biomed. Res. Int.* **2022**, 4230788 (2022). https://doi.org/10.1155/2022/4230788101155202242307 88
46. AlSheikh, H. M. A. et al. Plant-based phytochemicals as possible alternative to antibiotics in combating bacterial drug resistance. *Antibiotics* **9**, 480. https://doi.org/10.33073/pjm-2025-010 (2020).
47. Obukhova, E. S. & Murzina, S. A. Mechanisms of the antimicrobial action of fatty acids: A review. *Appl. Biochem. Microbiol.* **60**, 1035–1043. https://doi.org/10.1134/S0003683824605158 (2024).
48. Olowo-okere, A. et al. Phenotypic and genotypic characterization of clinical carbapenem-resistant Enterobacteriaceae isolates from Sokoto, northwest Nigeria. *New. Microbes New. Infect.* **37**, 100727. https://doi.org/10.1016/j.nmni.2020.100727 (2020).
49. Joujou, F. M., Darra, N. E., Rajha, H. N., Sokhn, E. S. & Alwan, N. Evaluation of synergistic/antagonistic antibacterial activities of fatty oils from apricot, date, grape, and black seeds. *Sci. Rep.* **14**, 6532. https://doi.org/10.1038/s41598-024-54850-y (2024).
50. Mráz, P. et al. Antibacterial activity and chemical composition of popular plant essential oils and their positive interactions in combination. *Molecules* **30**, 1864 (2025).
51. Andrade-Ochoa, S. et al. In vitro and in silico studies of terpenes, terpenoids and related compounds with larvicidal and pupaecidal activity against Culex quinquefasciatus Say (Diptera: Culicidae). *Chem. Cent. J.* **12**, 53. https://doi.org/10.1186/s13065-018-0425-2 (2018).
52. Dhanya, T. M. et al. Exploring the enzyme inhibition potential of schiff base and metal complexes of benzothiophene derivatives. *Discov Chem*. https://doi.org/10.1007/s44371-024-00048-0 (2024).
53. Che, T., Bethel, C. R., Pusztai-Carey, M., Bonomo, R. A. & Carey, P. R. The different inhibition mechanisms of OXA-1 and OXA-24 β-lactamases are determined by the stability of active site carboxylated lysine. *J. Biol. Chem.* **289**, 6152–6164. https://doi.org/10.1074/jbc.M113.533562 (2014).
54. Ersoy, S. C., Rose, W. E. & Proctor, R. A. Bicarbonate within: A hidden modulator of antibiotic susceptibility. *Antibiotics* **14**, 96 (2025).
55. Wang, E. et al. End-point binding free energy calculation with MM/PBSA and MM/GBSA: Strategies and applications in drug design. *Chem. Rev.* **119**, 9478–9508. https://doi.org/10.1021/acs.chemrev.9b00055 (2019).
56. Gazi, R., Maity, S. & Jana, M. Conformational features and hydration dynamics of proteins in cosolvents: A perspective from computational approaches. *ACS Omega*. **8**, 2832–2843. https://doi.org/10.1021/acsomega.2c08009 (2023).
57. Reeda, V. S. J. et al. Synthesis, functional group analysis (experimental and theoretical), solvent –Solute interactions, structural insights of (E)-3-(4-chloro-3-(trifluoromethyl) phenyl) imino) indolin-2-one–In-vitro Antimicrobial activity. *J. Mol. Struct.* **1294**, 136310. https://doi.org/10.1016/j.molstruc.2023.136310 (2023).
58. Ramírez-Velásquez, I., Bedoya-Calle, Á. H., Vélez, E. & Caro-Lopera, F. J. Shape theory applied to molecular docking and automatic localization of ligand binding pockets in large proteins. *ACS Omega*. **7**, 45991–46002. https://doi.org/10.1021/acsomega.2c02227 (2022).
59. Upmanyu, K., Haq, Q. M. R. & Singh, R. Factors mediating Acinetobacter baumannii biofilm formation: Opportunities for developing therapeutics. *Curr. Res. Microb. Sci.* **3**, 100131. https://doi.org/10.1016/j.crmicr.2022.100131 (2022).
60. Behzadnia, A., Moosavi-Nasab, M. & Oliyaei, N. Anti-biofilm activity of marine algae-derived bioactive compounds. *Front. Microbiol*. https://doi.org/10.3389/fmicb.2024.1270174 (2024).
61. Porras, M., Hernández, D. & Boto, A. Short synthesis of structurally diverse N-acylhomoserine lactone analogs and discovery of novel quorum quenchers against gram-negative pathogens. *Int. J. Mol. Sci.* **26**, 1775 (2025).
62. Ramanathan, S. et al. Biofilm inhibitory efficiency of phytol in combination with cefotaxime against nosocomial pathogen Acinetobacter baumannii. *J. Appl. Microbiol.* **125**, 56–71. https://doi.org/10.1111/jam.13741 (2018).
63. Rai, M. et al. Herbal concoction Unveiled: A computational analysis of phytochemicals' pharmacokinetic and toxicological profiles using novel approach methodologies (NAMs). *Curr. Res. Toxicol.* **5**, 100118. https://doi.org/10.1016/j.crtox.2023.100118 (2023).
64. Sohlenius-Sternbeck, A. K. & Terelius, Y. Evaluation of ADMET predictor in early discovery drug metabolism and pharmacokinetics project Work. *Drug Metab. Dispos.* **50**, 95–104. https://doi.org/10.1124/dmd.121.000552 (2022).
65. Scoffone, V. C., Barbieri, G., Irudal, S., Trespidi, G. & Buroni, S. New antimicrobial strategies to treat multi-drug resistant infections caused by gram-negatives in cystic fibrosis. *Antibiotics* **13**, 71 (2024).

Acknowledgements
None.

Author contributions
Muhammad Afzal carried out the experimental data including extraction, antibacterial experiments, GC–MS analysis and biofilm inhibition, and participated in the analysis of data and manuscript writing. Muhammad Umer Khan conceived and designed the study, supervised experimental and computational study aspects, validated results and contributed to manuscript writing, critical revision and correspondence. Syed Zeeshan Haider Naqvi supported the experimental design and GC–MS data interpretation, and biochemical characterization of *A. baumannii* in addition to reviewing the manuscript. Muhammad Kashif Munir conducted bacterial isolation, biochemical identification, and 16 S rRNA sequencing, and assisted with antimicrobial assays and data curation. Hasan Ejaz contributed to methodological refinement, supervision of analytical components, and critical review of biochemical and computational results. Muharib Alruwaili performed molecular docking, ADMET predictions, and contributed to the interpretation of molecular dynamics simulations. Bi Bi Zainab Mazhari assisted in computational analyses, DFT data interpretation, and manuscript editing. Lienda Bashier Eltayeb contributed to project administration, literature review, validation of findings, and final proofreading of the manuscript.

Funding
Not Applicable.

Declarations

Competing interests
The authors declare no competing interests.

Ethics approval and consent to participate
The University of Lahore's institutional ethics committee approved this research project.

Consent for publication
Not applicable.

Clinical trial number
Not applicable.

Additional information
Supplementary Information The online version contains supplementary material available at https://doi.org/10.1038/s41598-026-45012-3.

Correspondence and requests for materials should be addressed to M.U.K.

Reprints and permissions information is available at www.nature.com/reprints.

Publisher's note Springer Nature remains neutral with regard to jurisdictional claims in published maps and institutional affiliations.